

RESEARCH ARTICLE

10.1002/2017JD026888

Special Section:

Simulations of stratospheric sulfate aerosol geoengineering with the Whole Atmosphere Community Climate Model (WACCM)

This article is a companion to Mills et al. (2017), <https://doi.org/10.1002/2017JD027006>; Richter et al. (2017), <https://doi.org/10.1002/2017JD026912>; Kravitz et al. (2017), <https://doi.org/10.1002/2017JD026874>; and MacMartin et al. (2017), <https://doi.org/10.1002/2017JD026868>.

Key Points:

- Stratospheric SO₂ injections outside the equator at 25 km are more efficient in reducing global temperatures than at the equator
- Nonequatorial injections transport SO₂ more efficiently into middle and high latitudes and providing a larger region for aerosol formation
- Sufficiently large injections at the equator at different altitudes lead to similar climate impacts

Correspondence to:

S. Tilmes,
tilmes@ucar.edu

Citation:

Tilmes S., Richter J. H., Mills M. J., Kravitz B., MacMartin D. G., Vitt F., ... Lamarque J.-F. (2017). Sensitivity of aerosol distribution and climate response to stratospheric SO₂ injection locations. *Journal of Geophysical Research: Atmospheres*, 122, 12,591–12,615. <https://doi.org/10.1002/2017JD026888>

Received 31 MAR 2017

Accepted 22 SEP 2017

Accepted article online 6 NOV 2017

Published online 7 DEC 2017

Sensitivity of Aerosol Distribution and Climate Response to Stratospheric SO₂ Injection Locations

Simone Tilmes^{1,2} , Jadwiga H. Richter¹ , Michael J. Mills² , Ben Kravitz³ , Douglas G. MacMartin^{4,5} , Francis Vitt² , Joseph J. Tribbia¹ , and Jean-Francois Lamarque¹ 

¹Atmospheric Chemistry, Observations, and Modeling Laboratory, National Center for Atmospheric Research, Boulder, CO, USA, ²Climate and Global Dynamics Laboratory, National Center for Atmospheric Research, Boulder, CO, USA, ³Pacific Northwest National Laboratory, Richland, WA, USA, ⁴Mechanical and Aerospace Engineering, Cornell University, Ithaca, NY, USA, ⁵Department of Computing and Mathematical Sciences, California Institute of Technology, Pasadena, CA, USA

Abstract Injection of SO₂ into the stratosphere has been proposed as a method to, in part, counteract anthropogenic climate change. So far, most studies investigated injections at the equator or in a region in the tropics. Here we use Community Earth System Model version 1 Whole Atmosphere Community Climate Model (CESM1(WACCM)) to explore the impact of continuous single grid point SO₂ injections at seven different latitudes and two altitudes in the stratosphere on aerosol distribution and climate. For each of the 14 locations, 3 different constant SO₂ emission rates were tested to identify linearity in aerosol burden, aerosol optical depth, and climate effects. We found that injections at 15°N and 15°S and at 25 km altitude have equal or greater effect on radiation and surface temperature than injections at the equator. Nonequatorial injections transport SO₂ and sulfate aerosols more efficiently into middle and high latitudes and result in particles of smaller effective radius and larger aerosol burden in middle and high latitudes. Injections at 15°S produce the largest increase in global average aerosol optical depth and increase the change in radiative forcing per Tg SO₂/yr by about 15% compared to equatorial injections. High-altitude injections at 15°N produce the largest reduction in global average temperature of 0.2° per Tg S/yr for the last 7 years of a 10 year experiment. Injections at higher altitude are generally more efficient at reducing surface temperature, with the exception of large equatorial injections of at least 12 Tg SO₂/yr. These findings have important implications for designing a strategy to counteract global climate change.

1. Introduction

The continuous injection of SO₂ into the tropical stratosphere has been suggested as one of the most promising methods of climate engineering to modify the Earth's albedo and thus in part counteract global impacts resulting from increasing greenhouse gases (Committee on Geoengineering Climate, 2015; Crutzen, 2006; Schäfer et al., 2015). The injection of SO₂ into the stratosphere results in the formation of sulfate aerosols due to oxidation. Both SO₂ and the newly formed aerosols subsequently spread in longitude and are transported toward higher latitudes, driven by the stratospheric equator-to-pole circulation, also called the Brewer-Dobson circulation (BDC) (e.g., Andrews et al., 1987). Stratospheric tracer transport is further controlled by large-scale mixing and by transport barriers of the polar jets (Butchart, 2014).

Transport of aerosols into different areas of the globe has been observed after large volcanic eruptions, indicating that the resulting aerosol distribution strongly depends on the injection location and timing. For example, during the eruption of Mount Pinatubo in 1991, the injection of about 5 to 10 Tg sulfur (S) into the tropical stratosphere at a latitude of about 15°N led to an aerosol cover over low and middle latitudes after a couple of months and a global coverage including high southern latitudes after about 7 months (Aquila et al., 2013). Aerosol clouds from volcanoes that emitted SO₂ poleward of the subtropical jet stayed mostly in one hemisphere (Sakai et al., 2016).

In addition to transport, microphysical processes change the size and spatial distribution of aerosols. In contrast to volcanic eruptions where sulfur is injected into a clean background atmosphere, climate engineering applications continuously injecting SO₂ over many years result in an enhanced background aerosol layer. Newly formed particles coagulate with existing larger particles, which continuously increases the particle size with SO₂ emission amount. The resulting increase in sedimentation and reduced reflectivity of larger particles

leads to reduced scattering of sunlight and efficiency to cool the climate per Tg S injection (e.g., Kravitz et al., 2017; Niemeier & Timmreck, 2015; Vioni et al., 2017).

To investigate the impact and efficiency of SO₂ injections on the global climate, the inclusion of comprehensive processes in models is important, including stratospheric chemistry to simulate the formation of sulfate aerosols from SO₂ and their impact on chemical reactions. A parameterization of complicated aerosol microphysical processes to simulate formation, coagulation, condensational growth, lofting, evaporation, and sedimentation is required. Depending on aerosol size distribution and location, interactions with radiation and chemistry cause changes in temperature and chemical components including water vapor and stratospheric ozone (Pitari et al., 2014; Tilmes et al., 2009), which have impacts on surface climate (Marsh et al., 2013; Vioni et al., 2017). An internally generated quasi-biennial oscillation (QBO) is further required to include important interactions of stratospheric aerosols and dynamics (Shuckburgh et al., 2001). For instance, Aquila et al. (2014) demonstrated that enhanced stratospheric aerosol loading may significantly alter the QBO.

Earlier studies used simpler models without an aerosol microphysical model for simulating injections of SO₂ into the stratosphere (e.g., Rasch et al., 2008; Robock et al., 2008). Those simulations produced an unrealistically high burden of aerosols and therefore an unrealistic estimation of achieved radiative forcing reduction. Recent papers have addressed SO₂ and H₂SO₄ injection strategies using microphysical models (Aquila et al., 2014; English et al., 2012; Heckendorn et al., 2009; Hommel & Graf, 2011; Niemeier et al., 2011; Niemeier & Timmreck, 2015; Pierce et al., 2010). Some of these studies used a two-dimensional aerosol microphysical model to simulate the aerosol distribution of SO₂ or H₂SO₄ injections and then prescribed the aerosol distribution in a global climate model (GCM). Others used models that coupled aerosols and dynamics in the GCM, but none of those included interactions between aerosols, chemistry, and climate. Aerosols were injected right at the equator and also spread over a larger vertical region between 20 and 25 km and a larger horizontal region between 30°S and 30°N. It was shown that injections distributed evenly between 30°N and 30°S and additionally over an extended altitude region resulted in a spread of aerosols farther poleward (English et al., 2012; Pierce et al., 2010). Injection into higher altitudes were shown to be more efficient in producing a higher aerosol burden (Aquila et al., 2014; Niemeier & Timmreck, 2015). All these studies agree that increasing aerosol injections in the tropics will lead to increases in particle size and sedimentation and therefore reduced effectiveness with injection amount. The nonlinearity of the effective radiative forcing reduction with injection amount depends therefore on the injection strategy (e.g., English et al., 2012; Heckendorn et al., 2009; Niemeier et al., 2011).

Previous models used for SO₂ injection simulations did not include full coupling between aerosol microphysics, dynamics, chemistry, radiation, and climate (Pitari et al., 2014), and reasons for changing aerosol pattern with injection strategy have not been systematically explored. A detailed investigation of the effect of single injection locations at and outside the equator on the shape of the aerosol distribution and effectiveness of SO₂ injection on AOD and climate has not been performed to date. In this work, we perform for the first time a more comprehensive investigation of the impact of different SO₂ injection locations at 14 single injection locations in the stratosphere using a fully interactive model, as described in section 2. The newly developed Community Earth System Model version 1 Whole Atmosphere Community Climate Model CESM1(WACCM) with extensions described in Mills et al. (2016) includes all the above described processes interactively. This model reproduces the formation and lifetime of aerosols after recent volcanic eruptions very well (Mills et al., 2017). It also shows good agreement with observations in the forced response of radiation to past volcanic eruptions and is therefore well suited to use for the investigation of climate engineering processes using stratospheric sulfur injections. The goals of this study are (a) to assess the sensitivity of aerosol spatial distribution and radiative forcing to single-point SO₂ injection in the stratosphere at different latitudes and altitudes (sections 3.1 and 3.2), (b) to examine the linearity and efficiency of aerosol mass and size distribution and aerosol optical depth as a function of SO₂ injection amounts (section 3.3), and (c) to assess how the latitude and altitude of injection affect the impact on climate (section 4). Impacts on stratospheric dynamics and chemistry of these experiments will be investigated in a companion study (Richter et al., 2017). Building on the results of this study, companion studies (MacMartin et al., 2017; Kravitz et al., 2017) show how the combination of different SO₂ injection latitudes and amounts can be used to meet different climate objectives.

Table 1
Summary of the Single Injection Matrix of Simulations

Injection Latitude	50°S	30°S	15°S	Equator	15°N	30°N	50°N
Amount (Tg SO ₂ /yr)	6, 8, 12	6, 8, 12	6, 8, 12	6, 8, 12	6, 8, 12	6, 8, 12	6, 8, 12
Altitude (km)	12, 17	18, 23	20, 25	20, 25	20, 25	18, 23	12, 17

2. Model and Experimental Design

In this study we use CESM1(WACCM), a fully coupled Earth System model, which includes atmosphere, land, ocean, and sea ice components. This model version is based on CESM1 (Neale et al., 2013), with modifications discussed in Mills et al. (2017). Simulations were carried out on the Yellowstone high-performance computer platform (Computational and Information Systems Laboratory, 2012). The model horizontal resolution is 0.95° in latitude by 1.25° in longitude, with 70 vertical levels extending from the surface to 145 km. The configuration of the model used here fully couples the Community Atmosphere Model version 5 (CAM5), the Community Land Model version 4.0 (CLM4.0), the Parallel Ocean Program version 2 (POP2), and the Los Alamos sea ice model (CICE Version 4). The land model was run with interactive carbon and nitrogen cycles, and the atmospheric and land components are coupled to the chemistry. Biogenic surface emissions are calculated online in CLM using the Model of Emissions of Gases and Aerosols from Nature (MEGAN), version 2.1 (Guenther et al., 2012).

WACCM includes comprehensive stratospheric chemistry and an interactive modal treatment of tropospheric and stratospheric aerosols, including sulfate produced by natural and anthropogenic precursor gases. Stratospheric aerosol properties calculated in WACCM have been validated against a variety of observations spanning the period 1990–2014, which includes perturbations from large and moderate inputs of volcanic SO₂, as well as nonvolcanic background levels (Mills et al., 2016).

A control simulation was performed starting in 1975, with initialized land, ocean, and sea ice from the CESM1 transient simulation used for the large ensemble (LE) simulation (Kay et al., 2015) that does not include interactive stratospheric chemistry. The LE simulation started from a 402 year preindustrial control simulation, which provided a long spin-up for the ocean. For atmospheric initial conditions in 1975, we used results from the Chemistry-Climate Model Initiative (CCMI) simulations performed with an earlier version of WACCM (Garcia et al., 2017).

The control simulation is following historical emissions before 2000 and the Representative Concentration Pathway (RCP) 8.5 (Meinshausen et al., 2011) after the year 2000, with steadily increasing greenhouse gas concentrations through the year 2100, as described in Morgenstern et al. (2017). Results were evaluated based on observations, in particular, for the time after the eruption of Mount Pinatubo eruptions in 1991 (Mills et al., 2017). The radiative forcing response to volcanic eruptions good agreement with satellite observations. The model also reproduces other observed quantities well, including stratospheric winds and temperatures, water vapor and the slope of the tape recorder, phase and amplitude of the QBO, and total ozone including the evolution of the Antarctic ozone hole (Mills et al., 2017). This analysis points to reasonably well reproduced stratospheric dynamics. However, due to differences in the representation and tracer transport of different models, specifics of the aerosol distribution are expected to be model dependent and need to be addressed in a multimodel intercomparison study.

Starting from the control simulation in 2040, forty-two 10-year simulations were performed, over the period 2040 to 2049, that continuously injected a specific amount of SO₂ into a single grid point at one longitude (180°E) of the model in the stratosphere. Single grid point injections produce sulfate aerosols of smaller size that reflect sunlight more efficiently than injections over a longitude band (not shown). The experiments differ in altitude, latitude, and amount of annual SO₂ injections as shown in Table 1. Seven different latitude locations and two altitude locations were chosen, as well as three different amounts of injection. Simulations with injections that were performed at about 5 km above the tropopause are referred to as “high-altitude injection cases” in the following, and injections at about 1 km above the tropopause are referred to as “low-altitude injection cases,” consistent with earlier studies (English et al., 2012; Niemeier et al., 2011). Due to variations

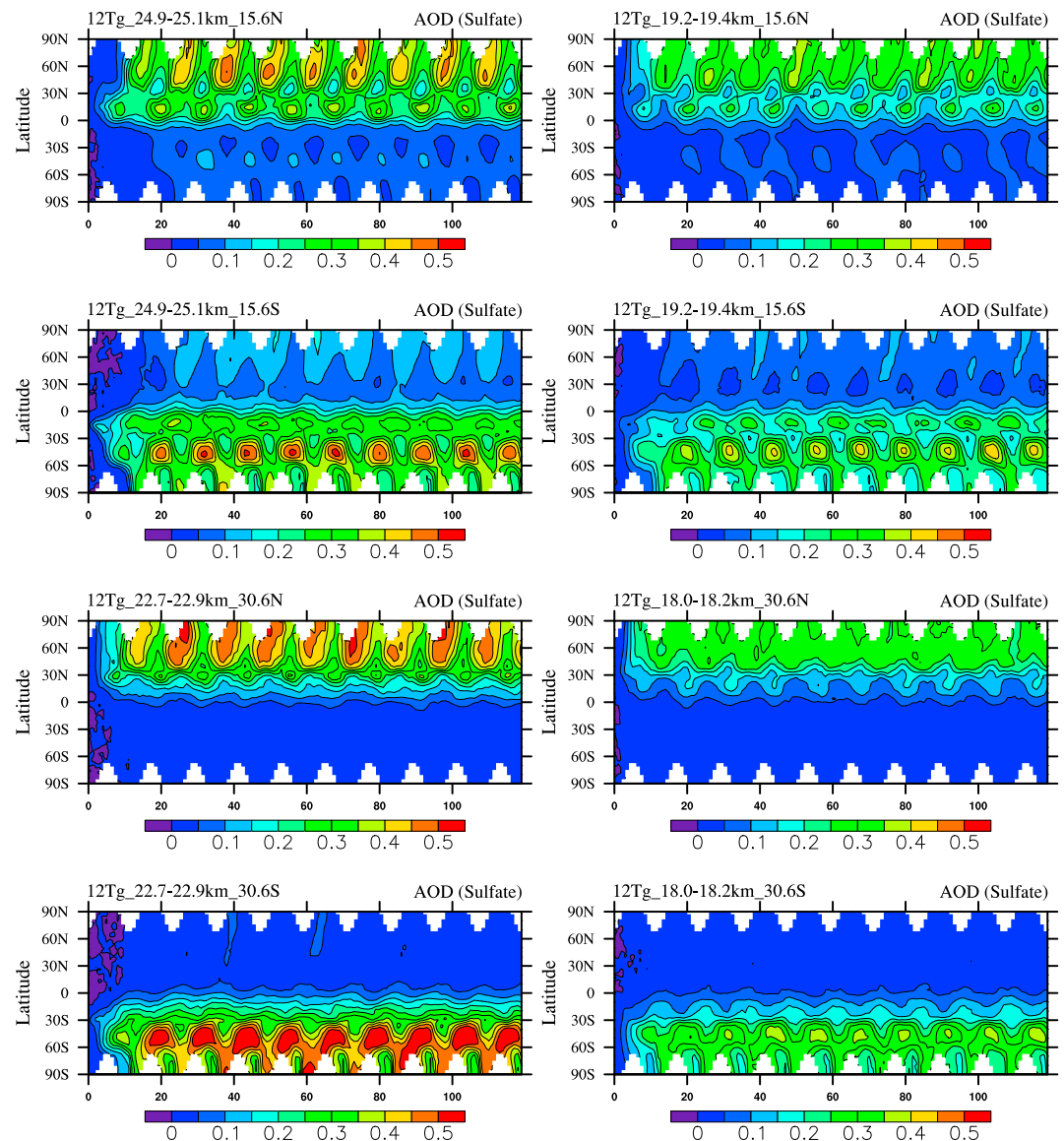


Figure 1. Aerosol optical depth in the visible (550 nm) from stratospheric sulfate for 12 Tg SO₂/yr injection simulations minus the control as a function of time (in months) for different injection locations, (first row) 15°N, (second row) 15°S, (third row) 30°N, and (fourth row) 30°S and injection altitude (left column) 5 km above the tropopause and (right column) 1 km above the tropopause.

of the tropopause altitude with latitude, injection locations vary between 17 km (50°N and 50°S) and 25 km (15°N and 15°S and the equator) for the high-altitude injection cases and 12 km (50°N and 50°S), and 20 km (15°N and 15°S and the equator) for the low-altitude injection cases. Annual injection amounts, distributed equally over the entire year, include 6, 8, and 12 Tg SO₂ per year.

The resulting patterns of enhancements in aerosol optical depth (AOD) are illustrated for different injection locations in Figure 1 and for different injection amounts at the equator in Figure A1. For all injection cases, AOD values increase for about 2 years until they reach a steady state distribution (see Figure A2, 12 Tg SO₂/yr equatorial injection case at 25 km) and produce a reoccurring seasonal pattern, as discussed in the following based on seasonal and annual averages over the period 2042–2049 for sulfate burden, AOD, and effective radius. Resulting temperatures continue to decline with time but show the strongest adjustments in the first 3 years (see Figure A2, bottom). Averages for surface temperature, precipitation, and top of the atmosphere imbalance are therefore averaged over the period 2043–2049.

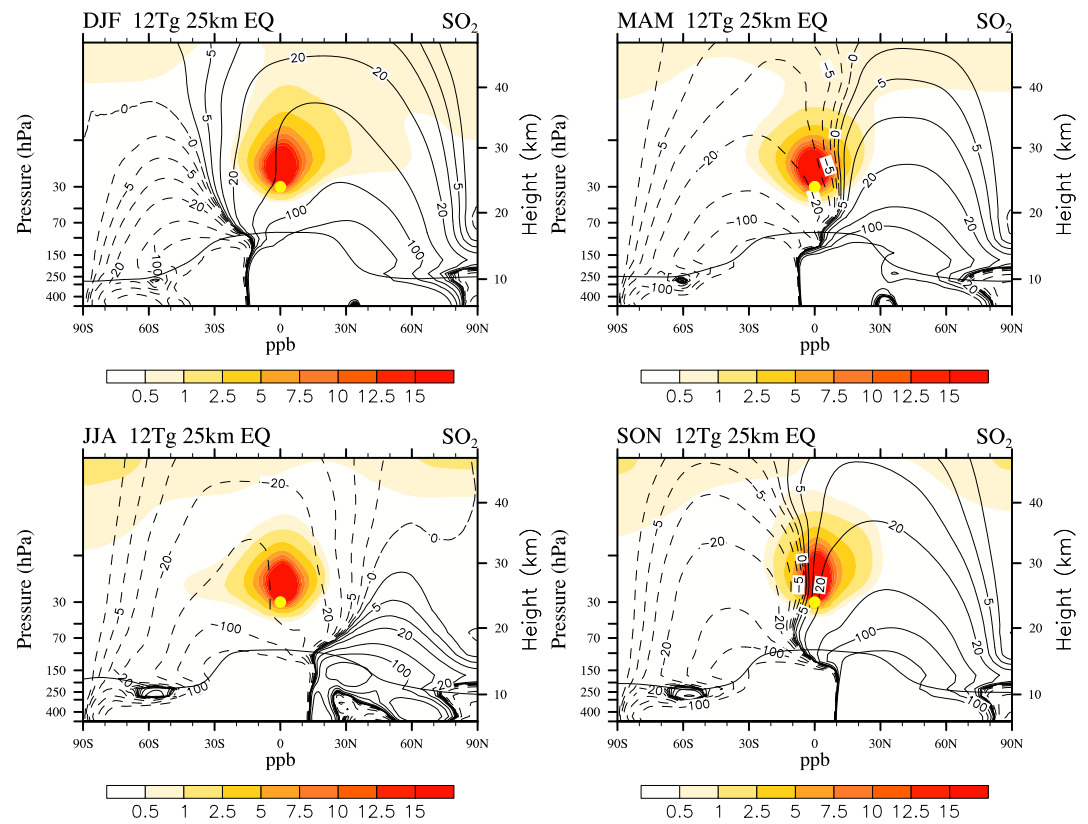


Figure 2. Seasonal zonal average SO_2 mixing ratios averaged between 2042 and 2049, (top left) December–February (DJF), (top right) March–May (MAM), (bottom left) June–August (JJA), and (bottom right) September–November, for the continuous injection of 12 Tg SO_2/yr at 25 km altitude at the equator (yellow dot), minus the control. Streamline averages of the TEM for the same period are indicated as black solid (positive) and dashed (negative) lines. The tropopause is indicated as a solid black line.

3. Distribution and Linearity of Sulfate Aerosols and the Effect on AOD

The steady state zonally averaged seasonal distribution of sulfate aerosols for different SO_2 injection locations and amounts is strongly controlled by the seasonal varying stratospheric transport driven by the Brewer-Dobson Circulation (BDC) and by large-scale mixing. The continuously injected SO_2 is advected toward different regions, depending on location and time (as discussed below), and oxidizes within about 45 days to form gas-phase H_2SO_4 , which very quickly nucleates to sulfate aerosols or condenses on existing aerosols. The formation and growth of sulfate aerosols are therefore dependent on the SO_2 distribution and the background aerosol concentration. Aerosols undergo further changes with time due to microphysical processes including self-coagulation and coagulation depending on the amount and size of already existing aerosols, evaporation, and lofting, sedimentation, and, once they reach the troposphere, removal through wet and dry deposition. Because of the nature of stratospheric transport and mixing, as described below, the production, size and removal of aerosols, and, therefore, its lifetime, strongly depend on the injection location.

The BDC is often illustrated as streamlines of the residual meridional circulation (see Figure 2), consisting of a deep branch in the tropics, lofting tracers upward and poleward into high altitudes with a lifetime of about 4–7 years. The deep branch is strongest in winter and spring of each hemisphere but stronger for the Northern Hemisphere (NH) than the Southern Hemisphere (SH) due to differences in the underlying topography, which change momentum deposition from gravity and planetary waves (e.g., Garcia and Randel 2008). The shallow branches are observed in both hemispheres throughout the year and result in transport of air masses from the lower tropical stratosphere directly toward the pole within a few months.

Streamlines of the transformed Eulerian mean (TEM) mass stream function are based on nongeostrophic eddy transport in the zonal mean flow (Plumb & Ferrari, 2005), as shown in Figures 2, 4, and 5, are projected onto the

SO₂ distribution (Figures 2 and 4) and onto the sulfate distribution (Figure 5) averaged between years 3 and 10 of the experiment. The divergence of the streamlines from positive (toward the NH) and negative (toward the SH) varies with time and alternates with season between about 30°S in December–February (DJF) and 30°N in June–August (JJA). Besides residual transport, tracers are also influenced by mixing and diffusion, which are not included in the illustration of streamlines. The mixing is driven by planetary Rossby waves, which occur primarily in winter in the so called “surf zone” between the subtropics and the polar jet stream, and by synoptic-scale waves above the subtropical jets (Butchart, 2014).

In the following sections, we investigate the SO₂ spatial distributions that result for different injection locations and discuss the difference between the single injection experiments and the control simulation, to illustrate locations where sulfate aerosol nucleation and condensational growth is expected. Differences in SO₂ and sulfate aerosol distributions with latitude for altitude injections at about 5 km above the tropopause are discussed in section 3.1. Those are contrasted with distributions resulting from altitude injections at about 1 km above the tropopause in section 3.2. The linearity of sulfate burden, AOD, and effective radius with injection amount is discussed in section 3.3.

3.1. Seasonality of SO₂ and Sulfate Aerosol Distributions for Injections 5 km Above the Tropopause

3.1.1. Tropical Injections

For injections at the equator, shown in Figure 2, enhanced SO₂ mixing ratios are mostly distributed between 30°N and 30°S and at altitudes between 25 and 30 km for all seasons, due to the upward transport of SO₂ following the deep branch of the BDC. This is leading to the formation of sulfate aerosol mostly in the tropics and sedimentation of aerosols into altitudes below the injection location. As a result of these processes, the sulfate aerosol distribution (Figure 3, top) shows a maximum stratospheric sulfate burden at the equator, a minimum around 25–30°N and 25–30°S, and a secondary maximum around 40–50°S and 50–60°N, in winter and spring of each hemisphere, with the secondary maximum being less than half as high as in the tropics (Figure 3, top). The distribution is strongly controlled by the containment of aerosol particles within the tropical pipe and the large-scale mixing in winter and spring midlatitudes in each hemisphere causing rapid transport of sulfate aerosols away from the tropics creating a minimum at 25–30°N and 25–30°S. Horizontal mixing is more strongly limited between middle and high latitudes in the SH in winter and spring than in the NH, due to the existence of a stronger polar vortex in the SH. This leads to larger aerosol mass burden in the SH midlatitudes in June–August and September–November. A small enhancement of SO₂ compared to the control simulation occurs in both hemispheres above about 20 hPa (Figure 2) and is the result of photolysis of sulfuric acid after the evaporation of enhanced sulfate aerosol at these altitudes for the injection experiments.

3.1.2. 15°N/15°S Injection

The SO₂ distribution of injections at 15°N and 15°S and at 5 km above the tropopause is very different from the tropical injection case (Figure 4). In summer of the injection hemisphere (DJF for 15°S), the SO₂ pattern indicates that tracers have been following the deep branch of the BDC, showing SO₂ mixing ratios extended upward and slightly across the equator toward the opposite hemisphere of the injection location. This transport is stronger for injections in the SH than in the NH, since the transport of the BDC is stronger toward the NH in winter and spring. Based on the location of enhanced SO₂ mixing ratios in a region close to the injection location, a maximum in sulfate mass burden can be found in that region as well (Figure 5, top left). Existing enhanced sulfate burden that is located poleward of the divergence point is further transported toward the pole of the injection hemisphere, which results in a secondary maximum in DJF (Figure 3, second row, left panel).

For 15°S in winter (JJA), the divergence of streamlines has moved away from the injection location (Figures 4 and 5). Mixing in the surf zone causes SO₂ and sulfate aerosols to be distributed throughout the tropics and midlatitudes of the injection hemisphere, while the polar jet blocks further transport toward the pole at around 60°, which results in a second and larger maximum in winter and spring (JJA and SON) (Figure 3, second row, left panel). This maximum is only about 10% smaller than the tropical peak for the injection at the equator for high-altitude injections. The shape of the aerosol distribution differs for injections at 15°N and at 15°S. More sulfate burden is simulated for injections in the SH than in the NH due to differences in the strength of the polar vortex and mixing.

3.1.3. 30°N/30°S and 50°N/50°S Injections

For the 30°N/30°S injections, SO₂ is injected into the subtropical lower stratosphere. Therefore, SO₂ and sulfate aerosol are mostly impacted by isentropic mixing within the injection hemisphere and only in summer

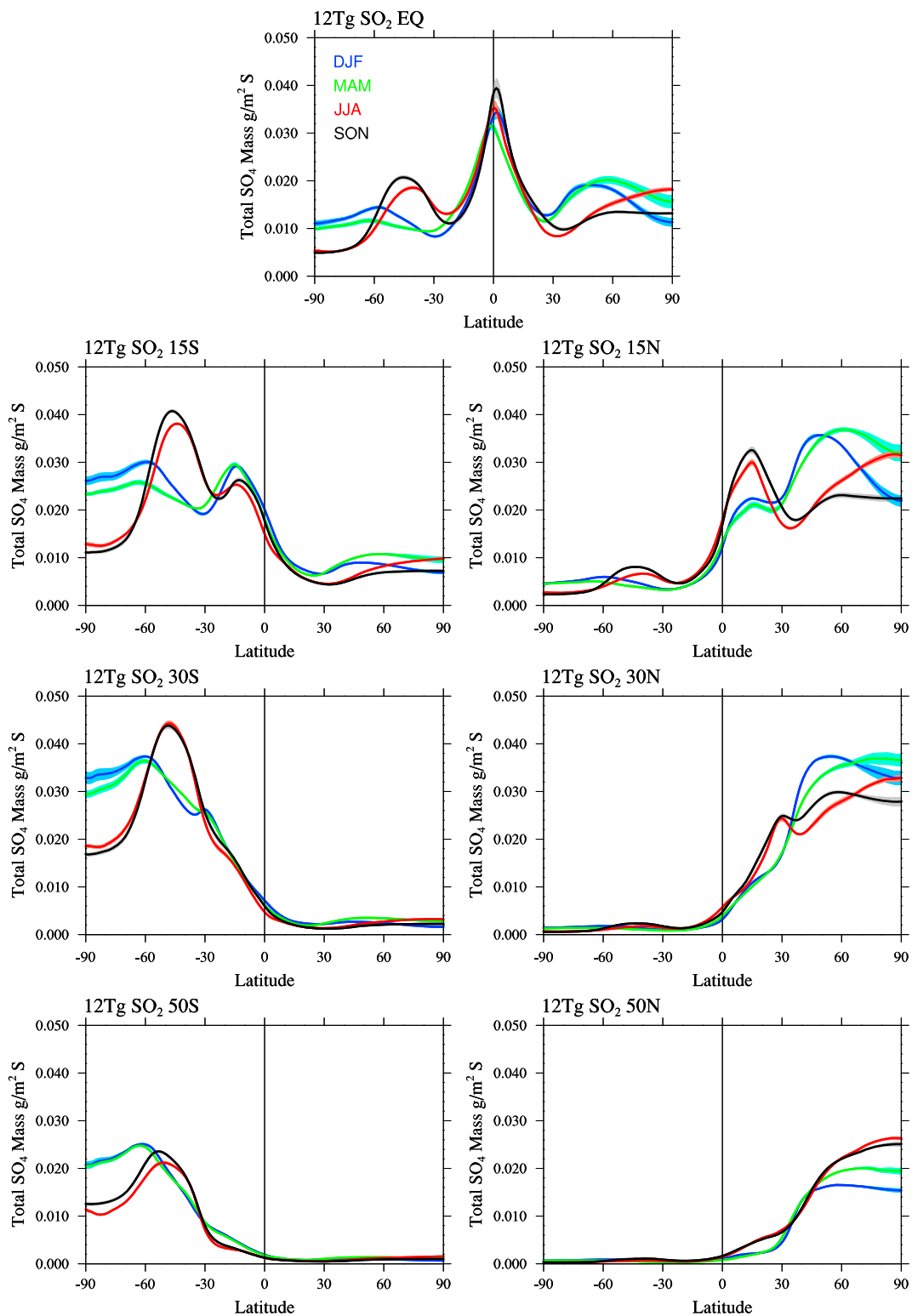


Figure 3. Seasonal zonal averaged stratospheric sulfate total mass burden ($\text{g/m}^2 \text{ S}$) averaged between 2042 and 2049, December–February (DJF) (blue), March–May (MAM) (green), June–August (JJA), (red), and September–November (SON) (black), for the continuous injection of 12 Tg SO_2/yr at different locations for high-altitude injections, only (different panels), minus the control. Variability within different years in terms of standard deviation is indicated as shaded regions around the lines.

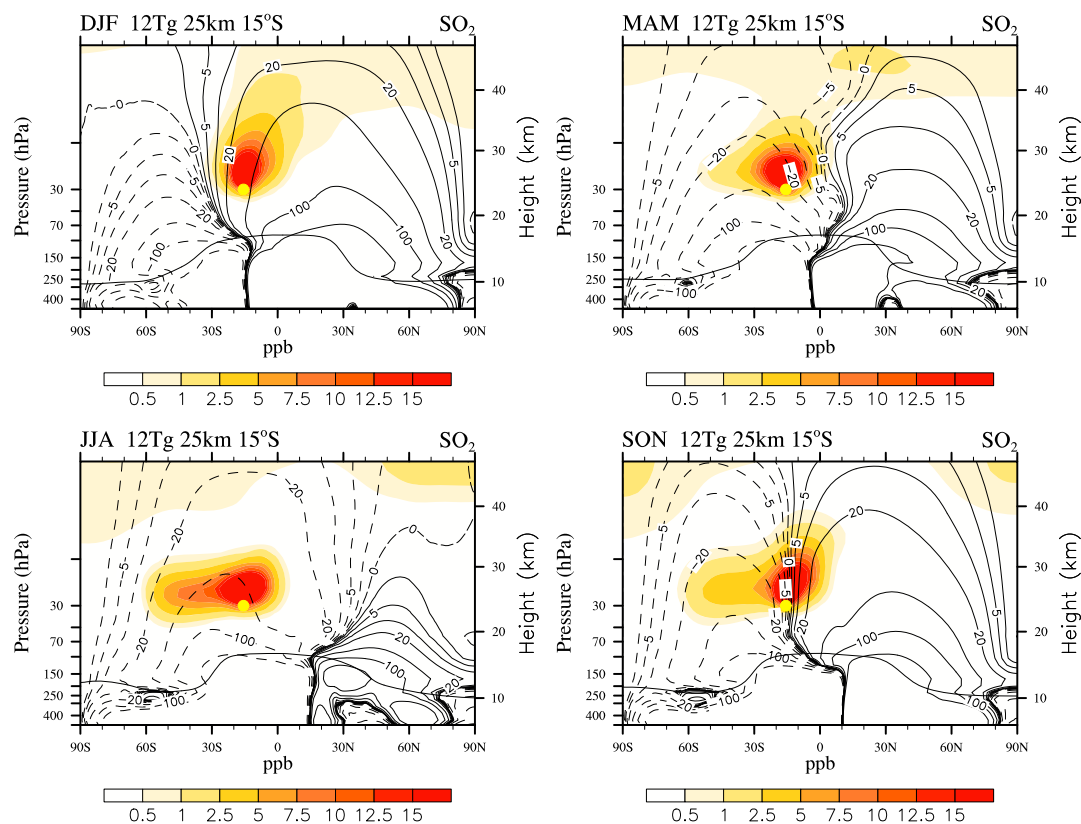


Figure 4. Same as Figure 2 but for continuous injections of 12 Tg SO₂/yr at 25 km altitude at 15°S.

impacted by the deep branch of the BDC (Figure A3). Almost no enhancement in aerosol mass compared to the control simulation can be found at the opposing injection hemisphere for the 30°N and 30°S injection cases. As for the 15°N and 15°S injection, the sulfate aerosol distribution peaks in winter and spring at middle and high latitudes for the 30°N injection, while for the SH, the polar vortex blocks tracer transport at around 60°S and therefore results in a larger maximum in midlatitudes than for the NH injection. This results in a 20% larger peak in sulfate mass for the 30°S high-altitude injection case than for the 30°N injection and is also larger than the tropical peak of injections at the equator (Figure 3, third row).

High-altitude injections at 50°N and 50°S and at 17 km result in similar SO₂ distributions to the 30°N/30°S distribution. However, the SO₂ distribution is concentrated poleward of 30° of the injection hemisphere, since the injection location always poleward of the subtropical jet (not shown). Since aerosols are located closer to the shallow branch and downward directed streamlines of the BDC, the removal of tracers is faster and the aerosol mass is about 30–40% lower than for the 30° injections for each injection hemisphere.

In summary, injections 15° or farther away from the equator allow SO₂ and sulfate aerosol to be transported more effectively toward middle and high latitudes up to 10°S to 60°S, allowing for additional nucleation and condensational growth in that region. Varying injection locations with season could be a way to increase the aerosol formation region, which would influence the size of the aerosols and the sulfate mass distribution. However, due to the lifetime of sulfate, seasonal variations are also strongly controlled by residual stratospheric transport, transport barriers, and mixing.

3.2. Sulfate Mass Distribution for Injections at About 1 km Above the Tropopause

The injection at 5 km above the tropopause, as discussed in section 3.1, results in annually averaged aerosol distributions that cover altitudes between the tropopause and up to 35 km (about 100–15 hPa) in the tropics (Figure 6). For the low-altitude injection cases, at about 1 km above the tropopause, most of the enhanced stratospheric sulfate mass is located between the tropopause and 25 km (25 hPa) (Figure 7) and produces a shallower aerosol distribution in the stratosphere than for the high-altitude injection cases. The peak of the sulfate mass for injections at the equator (Figure 8, top, middle panel) is much smaller for the low-altitude

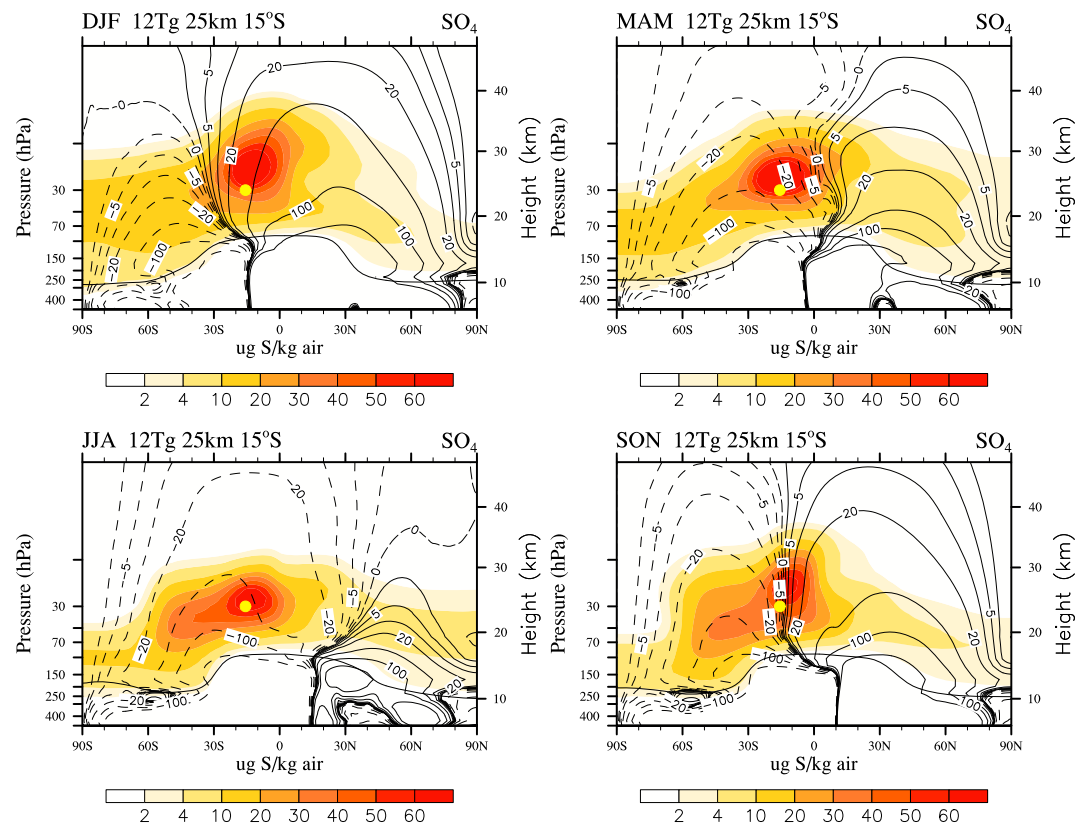


Figure 5. Seasonal zonal average sulfate mixing ratios ($\mu\text{g S/kg air}$) averaged between 2042 and 2049, (top left) December–February (DJF), (top right) March–May (MAM), (bottom left) June–August (JJA), and (bottom right) September–November (SON), for the continuous injection of 12 Tg SO_2/yr at 25 km altitude at 15°S (yellow dot), minus the control. Streamline averages of the TEM for the same period are indicated as black solid (positive) and dashed (negative) lines. The tropopause is indicated as a solid black line.

injection cases (solid lines) than for the high-altitude injection cases (dashed lines), while the changes in middle and high latitudes are comparable. This is because for the high-altitude injection case aerosols mostly remain in the tropics and grow larger, while for the low-altitude injections aerosols are moved faster toward midlatitudes.

For the 15°N and 15°S injection cases (Figure 8, right and left columns), the shapes of the sulfate mass distribution for low- and high-altitude injection cases are very similar. However, the amount for sulfate mass is up to 50% larger for the high injection cases including the peak of sulfate mass at the injection location. Since the location of the injection is lower, a larger fraction of tracers is influenced by the airflow of the shallow branch of the BDC. As for the injections at the equator, this results in a faster transport of SO_2 toward high latitudes. The injections at 30°N and 30°S are less efficient in accumulating sulfates for the low-altitude injection cases compared to the high-altitude injection cases, and almost no sulfate remains in the stratosphere for the 50°N and 50°S injection cases (Figure A4). Differences in aerosol distribution also impact the temperature response, which changes stratospheric transport and condensation and evaporation of aerosols. A detailed discussion on differences between high and low injection locations for combined injections at 15°N and 15°S injection will be performed in future studies.

3.3. Sulfate Lifetime and AOD Changes With Injection Amount

In this section, we explore the dependency of stratospheric sulfate lifetime and AOD with injection amount at different injection locations and therefore identify injection locations that are more efficient than others to influence radiation and climate. In addition, depending on the injection location, relative changes in global sulfate aerosol and AOD with increasing injection amount are not linear and the ability to manipulate AOD with changes in sulfate burden therefore also depends on the injection amount.

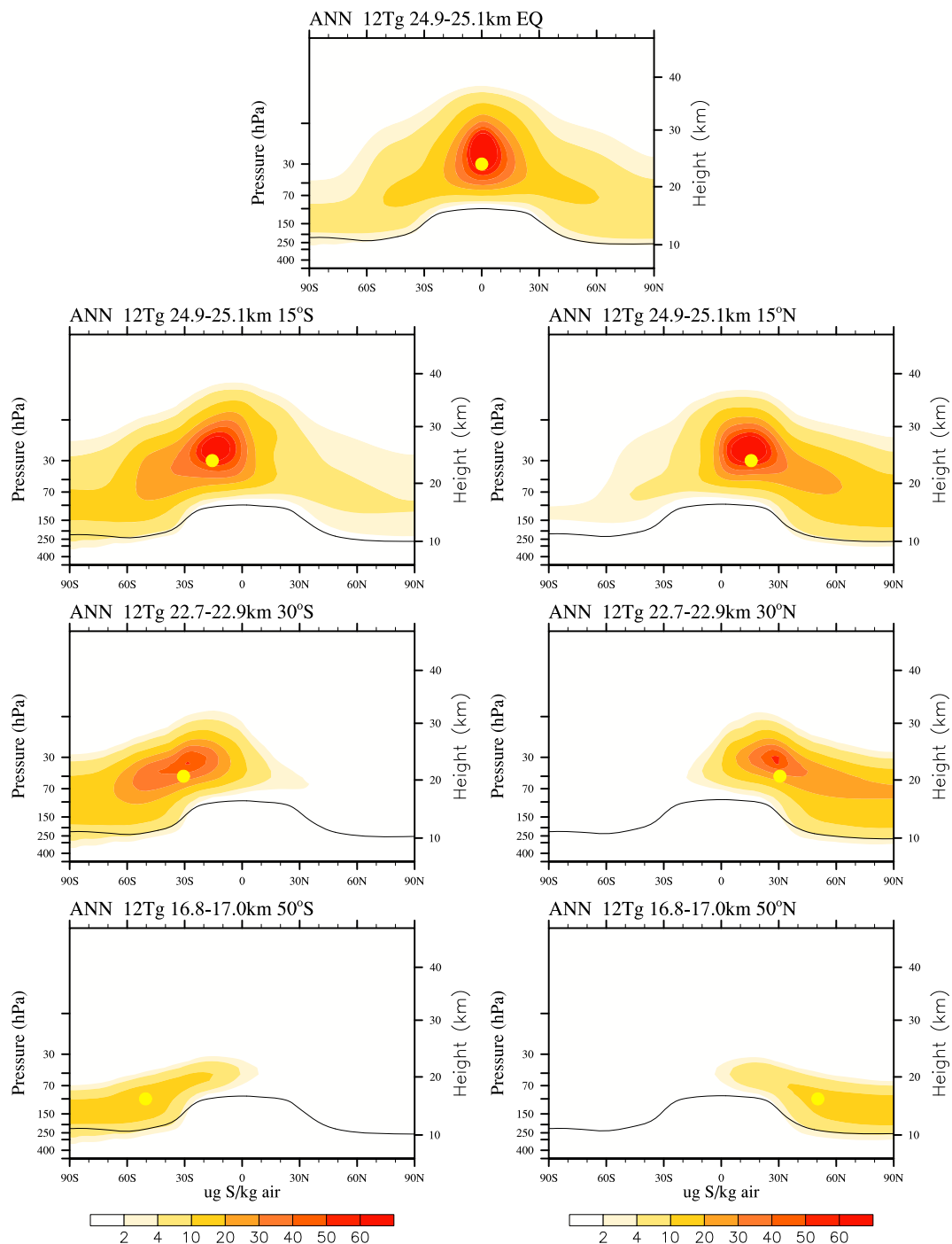


Figure 6. Stratospheric sulfate mass mixing ratio ($\mu\text{g S/kg air}$), 2042–2049 annual averages minus the control simulation for the same period, for the 12 Tg SO_2 injection cases at (top) 5 km above the tropopause at the equator, at (second row) 15°S (left) and 15°N (right), at (third row) 30°S (left) and 30°N (right), and at (fourth row) 50°S (left) and 50°N (right). All differences are significant at the 5% level. The injection location is illustrated as a yellow point in each panel, and the averaged location of the tropopause from the injection simulation is shown in black.

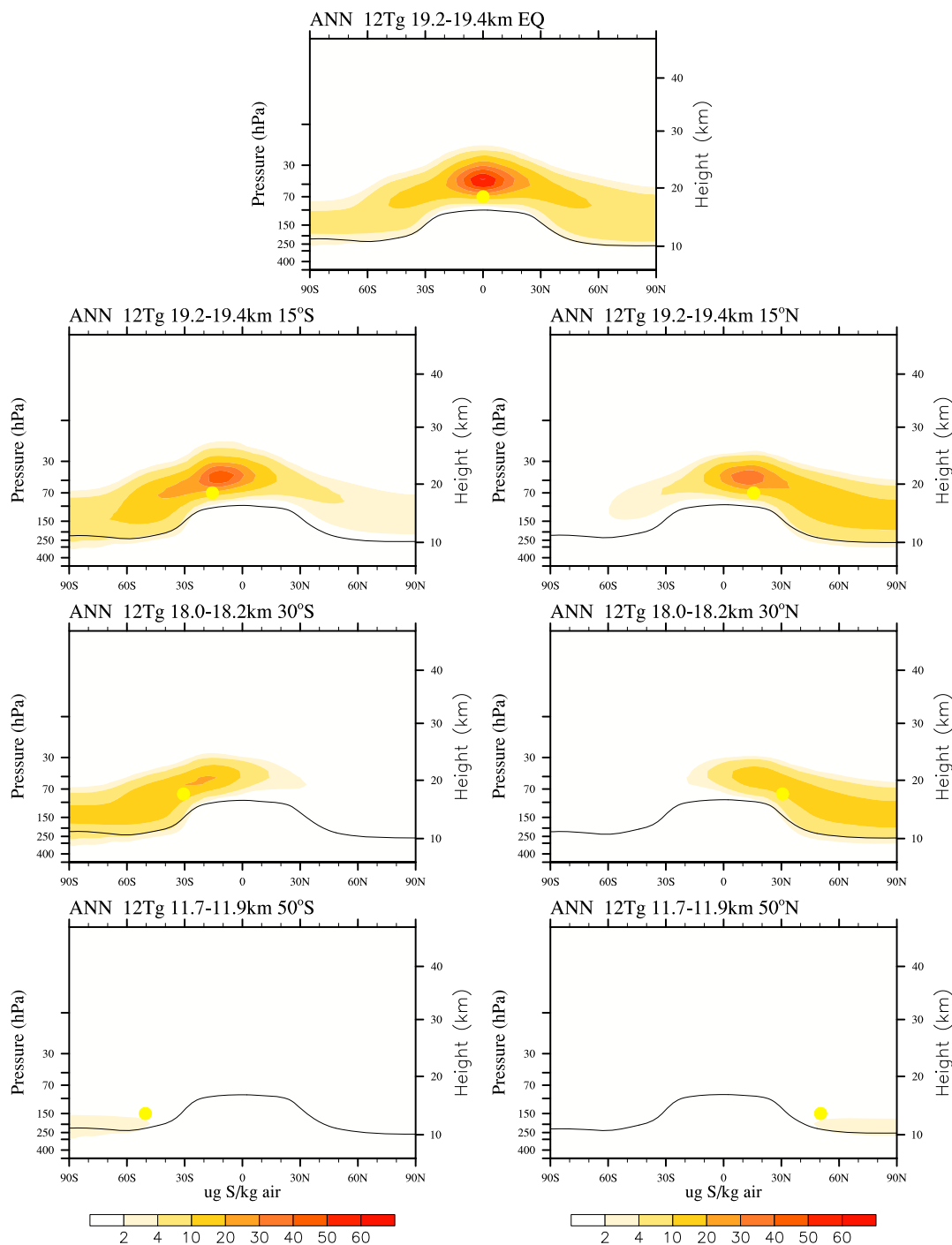


Figure 7. Same as Figure 6 but for the 12 Tg SO₂ injection cases at 1 km above the tropopause

3.3.1. Zonal Changes in SO₄ Burden and AOD for Different Injection Cases

Increasing amounts of SO₂ injections at the equator result in a large increase in the peak value of sulfate burden in the tropics for high-altitude injection cases (Figure 8, first row, middle panel). In contrast, low-altitude injections result in a relatively smaller increase in the peak at the equator, as discussed above, and a similar increase in middle and high latitudes compared to the high-altitude injection cases. AOD follows a similar pattern to the zonally averaged sulfate distribution for the different injection cases (Figure 8, second row). However, peaks in the sulfate distribution are relatively larger than peaks in the zonal AOD distribution, in particular, for the high-altitude injection cases at the equator. This is because AOD is dependent on the size

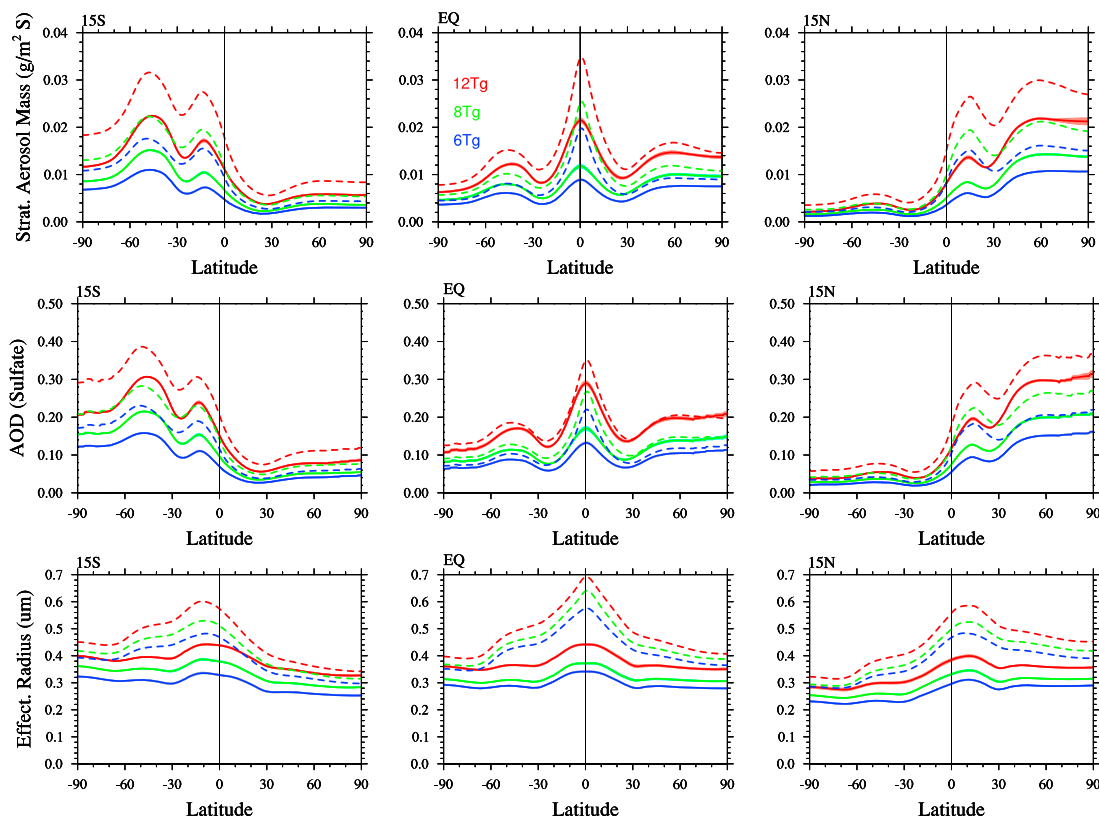


Figure 8. Annually and zonally averaged (top row) stratospheric sulfur mass, (middle row) aerosol optical depth from sulfate aerosols, minus the control, and (bottom row) effective wet radius weighted by surface area density for different injection locations, 15°S (left column), equator (middle column), and 15°S (right column), different injection altitudes, 1 km above the tropopause (solid lines) and 5 km above the tropopause (dashed lines), and for different injection amount, 6 Tg SO₂/yr (blue), 8 Tg SO₂/yr (green), 12 Tg SO₂/yr (red).

distribution and the effective radius of sulfate particles, since larger values of effective radius for the same mass result in reduced scattering of light and therefore reduced AOD per sulfate burden.

The largest effective radius values are simulated at the SO₂ injection location, where nucleation, coagulation, and condensational growth on existing background aerosols is expected to be largest. The enhanced background aerosols are largest for high-altitude injections at the equator (Figure 8, third row). For injections at the equator and at 15°N and 15°S, the size of the effective radius declines toward the poles (Figure 8, third row). For the 30° and 50° injection cases, the effective radius is more similar for the entire injection hemisphere (Figure A4), since condensational growth occurs over a larger region. For the low-altitude injection locations, the effective radius is smaller and does not vary nearly as much with latitude. Therefore, low-altitude injection cases result in a larger change in AOD per sulfate burden change than for the high-altitude injection cases.

3.3.2. Linearity of Sulfate Lifetime and AOD per Injection Amount

In the following discussion, we discuss changes of global stratospheric sulfate lifetime and AOD changes per injection amount with regard to injection location and amount (Figure 9 and Tables 2 and 3). The stratospheric lifetime is defined as the global stratospheric aerosol burden in Tg S divided by the injection rate in Tg S/yr.

The injection at high altitudes (5 km above the tropopause) results in about 50% larger mass burden in the stratosphere due to an increase in vertical extent of the aerosol particles and less removal due to a longer sedimentation path compared to the low-altitude injection case (Figure 9, top row). On the other hand, with increasing SO₂ injection amount, the lifetime of sulfate decreases for the high-altitude injection cases, especially for injections at the equator and at 15°N and 15°S by around 8% between 6 and 12 Tg SO₂ injections per year (see Table 2). The main factor is the increase in effective radius with emission amount for high-altitude injection cases, in particular, for the injection at the equator, which results in a faster removal of aerosol mass. The stratospheric sulfate lifetime is largest for injection at 15°S, while it is larger for injections at the equator

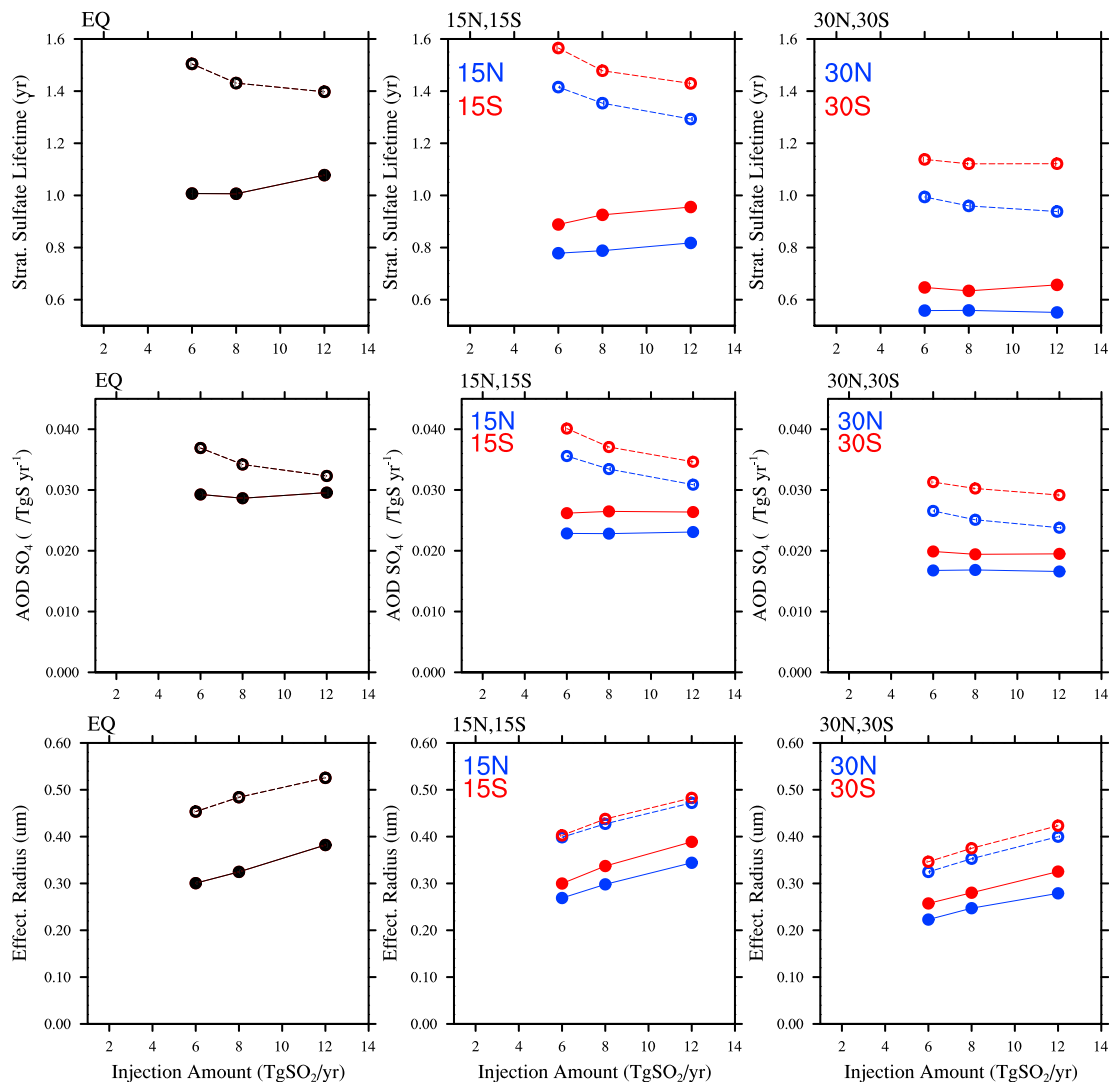


Figure 9. Annually and globally averaged (top row) stratospheric sulfate mass, (middle row) aerosol optical depth from sulfate aerosols, minus the control and divided by the injection amount, and (bottom row) effective wet radius weighted by surface area density, shown for different injection amounts and for different injection altitudes, 1 km above the tropopause (solid lines and filled circles) and 5 km above the tropopause (dashed lines and open circles), and for different regions (different columns). The uncertainty of global values due to natural variability in both the injection and control simulations is less than 2%.

than injections at 15°N (Table 2). This is due to differences in the transport of SO₂ and sulfate aerosols into different hemispheres.

In contrast, for the low-altitude injection case, sulfate lifetime is not decreasing with injection amount but is actually increasing from 8 to the 12 Tg SO₂ per year injections, despite the fact that global-averaged aerosol effective radius is larger. This is because the effective radius grows more equally over all latitudes (Figure 9, bottom row), since more aerosols are transported outside the tropics, which likely results in reduced sedimentation compared to the high-altitude injection case. The wet effective radius for the low injection cases reaches values up to 0.45 μm, compared to up to 0.7 μm for the high injection cases at the equator (Figure 8, bottom and middle rows). Furthermore, the aerosol lifetime is larger for injections at the equator than outside the equator (Table 2). In this case, the effective radius is similar for both injections at the equator and at 15°N and 15°S.

Difference in normalized AOD changes between high- and low-altitude injections are in general much smaller than differences in the sulfate lifetime (Table 3 and Figure 9, middle row), as a result of the differences in the effective radius. AOD per injection amount decreases with high injection rates for the high-altitude cases but does not change for the low-altitude injections. For the injections at the equator, high injection rates become

Table 2
Stratospheric Sulfate Lifetime (Year) With Injection Latitude, Derived Between 2042 and 2049

Altitude	Injection	50°S	30°S	15°S	Equator	15°N	30°N	50°N
30 hPa	6 Tg SO ₂	0.51	1.14	1.56	1.50	1.41	0.99	0.44
30 hPa	8 Tg SO ₂	0.51	1.12	1.48	1.44	1.36	0.96	0.43
30 hPa	12 Tg SO ₂	0.51	1.12	1.43	1.41	1.33	0.94	0.43
60 hPa	6 Tg SO ₂	0.04	0.65	0.89	1.01	0.78	0.56	0.05
60 hPa	8 Tg SO ₂	0.04	0.64	0.92	1.00	0.79	0.56	0.04
60 hPa	12 Tg SO ₂	0.04	0.66	0.95	1.07	0.82	0.55	0.04

Note. Uncertainty is less than 2% for all cases.

less effective with injection amounts, leading to only about 7% larger normalized AOD values for the high- compared to the low-altitude injection case for 6 Tg S per year. As for the equatorial injections, normalized AOD values also differ less between high- and low-altitude injections with increasing injection amount for injection outside the equator. Changes in AOD per injection amount are largest for injections at 15°S and similar for injections at the equator and injections at 15°N for high-altitude injections, while they are largest for injections at the equator for low-altitude injections.

In conclusion, the injection at lower altitudes results in smaller particles, which scatter more sunlight than larger particles and therefore are more efficient in reducing AOD for the same amount of mass. On the other hand, for the low-altitude injection cases, transport through the lower branch of the BDC moves aerosols faster toward high latitudes, where they are more quickly removed from the stratosphere compared to the high-altitude injections for the same injection amount. Low-altitude injections at the equator lead to the largest sulfate lifetime, while high-altitude injections lead to largest sulfate lifetime outside the equator. The difference between AOD per injection amount for high and low injections at the equator is more similar than outside the equator and values become more similar with increasing injection amount.

4. Climate Response

4.1. Zonal Changes in Climate Variables for Different Injection Cases

The increase in AOD as discussed above results in reduced incoming solar radiative flux. This changes the energy budget and, with this, the residual top of the atmosphere (TOA) radiative imbalance. TOA imbalance is defined as the difference between net short-wave (SW) and net long-wave (LW) radiation. It therefore takes into account changes in the SW radiation, including reductions as a result of increase in AOD, adjustments of clouds, and seasonality of sunlight and surface albedo, in particular, from changes in sea ice. Furthermore, changes in the long-wave radiation are a result of changes in clouds, adjustments in greenhouse gases including water vapor, ozone, and atmospheric and surface temperatures. Changes in the TOA imbalances are therefore not directly related to change in stratospheric AOD and vary strongly with latitude (Figure 10, second row).

Table 3
AOD Change per Tg S/yr With Injection Latitude, Derived Between 2042 and 2049

Altitude	Injection	50°S	30°S	15°S	Equator	15°N	30°N	50°N
30 hPa	6 Tg SO ₂	0.016	0.031	0.040	0.037	0.036	0.027	0.013
30 hPa	8 Tg SO ₂	0.016	0.030	0.037	0.034	0.033	0.025	0.013
30 hPa	12 Tg SO ₂	0.016	0.029	0.035	0.032	0.031	0.024	0.013
60 hPa	6 Tg SO ₂	0.002	0.020	0.026	0.029	0.023	0.017	0.002
60 hPa	8 Tg SO ₂	0.002	0.019	0.027	0.029	0.023	0.017	0.002
60 hPa	12 Tg SO ₂	0.002	0.020	0.026	0.030	0.023	0.017	0.002

Note. Uncertainty is less than 2% for all cases.

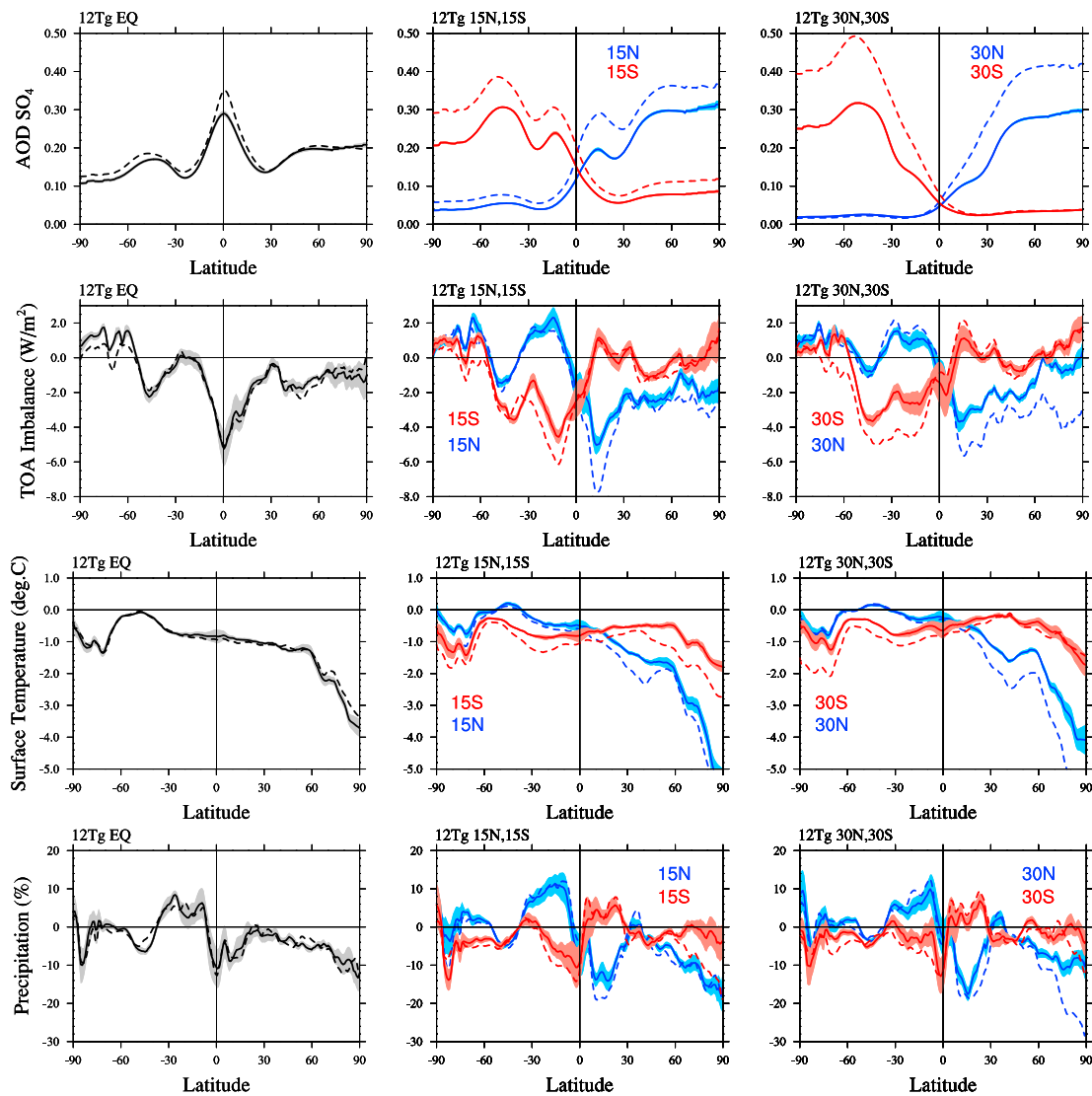


Figure 10. Annually and zonally averaged (first row) aerosol optical depth from sulfate aerosols, (second row) TOA imbalance, (third row) surface temperature, and (fourth row) precipitation, minus the control, for different injection locations, (left column) equator, (middle column) 15°N and 15°S, and (right column) 30°N and 30°S, and different injection altitudes, 1 km above the tropopause (solid lines) and 5 km above the tropopause (dashed lines), using an injection of 12 Tg SO₂/yr for all cases.

The large increase in AOD for tropical SO₂ injections (Figure 10, top left) results in a reduction in the TOA imbalance relative to the control simulation, which is largest in the tropics with a minimum in midlatitudes and small changes in high latitudes. On the other hand, for the 15°N and 15°S and 30°N and 30°S injection cases, the largest AOD increase occurs around 40–60°S for the corresponding injection hemisphere and stays high toward the poles. The largest changes in TOA imbalance are, however, found closer to the tropics especially for the 15°N and 15°S injection cases, with rather small changes at high latitudes. Reduced sunlight in high latitudes results in reduced effectiveness of AOD changes on the TOA imbalance in high latitudes. In addition, changes in clouds play an important role. Tropical precipitation (Figure 10, bottom row) and therefore convective systems and clouds shift toward the opposing hemisphere of the injection hemisphere (Haywood et al., 2013). This results in a decrease of the TOA imbalance poleward of the equator in the injection hemisphere and an increase in the opposing hemisphere. For the injections at the equator, some shift in precipitation from NH to SH tropics is likely the result of a stronger increase of AOD in the NH.

For the 15°N and 15°S cases, the largest differences in the TOA imbalance occur close to the tropics, where the largest changes in precipitation and clouds have occurred (Figure 10, bottom row). The largest differences

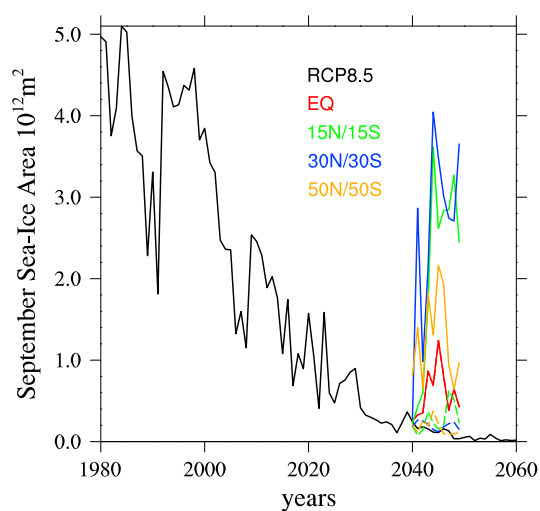


Figure 11. September Arctic sea ice area for the CESM1(WACCM) control simulation (black) and for different injection scenarios considering only 12 Tg SO₂/yr injections. The NH injection cases are shown as solid lines; the SH injection cases are shown as dashed lines.

between high- and low-altitude injection locations is found for the 30°N and 30°S injection cases, with a significant reduction in TOA imbalance over all latitudes in the injection hemisphere. These reductions reach values similar to the tropical values for injections at the equator.

Zonal mean changes in the TOA imbalance do not directly translate to zonal mean temperature changes (Figure 10, third row). For injections at the equator and injections in the NH, the strongest reductions in temperature occur in high northern latitudes, counteracting the large winter warming in northern high latitudes as a result of increasing greenhouse gases (Figure A5). The cooling in the tropics and midlatitudes is a major driver for reducing the atmospheric and oceanic heat transport to the Arctic, as discussed by Tilmes et al. (2014). This results in reducing the winter warming of the Arctic caused by increasing greenhouse gases in an RCP8.5 scenario, even for injections in the SH. The cooling effect is significantly stronger in the NH, where the TOA imbalance is reduced more strongly in the NH middle and high altitudes than in the SH. A contributing factor to the cooling in the NH is also the recovery of the summer Arctic sea ice (Figure 11). Arctic September sea ice has grown back to about 2010 values for the 15°N and 30°N injections. Besides the reduced heat transport from atmosphere and ocean, the direct reduction of incoming sunlight in the high injection cases compared to the low injection cases results in further reductions in surface temperatures.

Very little cooling is achieved over the Southern Ocean around 55°S for all injection case, including for the injection in the SH (Figure A6). The short period of the experiment covering only 10 years is not sufficient to have a strong cooling effect in the Southern Ocean. Surface temperatures over the Southern Ocean and over middle and high northern latitudes show increased cooling for an extended injection experiment over 20 years, as shown by MacMartin et al. (2017, Figure 1). An additional reason for the reduced cooling over the Southern Ocean may be changes in the location of the SH polar vortex with SO₂ injections, as described by Richter et al. (2017). A shift in the Antarctic polar vortex as a result of sulfur injections can lead to a warming belt in the Southern Ocean and therefore a warming rather than a cooling, as discussed by McCusker et al. (2015).

4.2. Linearity of Climate Variables to Injection Amount

The efficiency and linearity of globally averaged TOA imbalance, surface temperature, and precipitation changes with injection amount are illustrated in Figure 12 for different single injection locations and listed in Tables 4 and 5. Here we illustrate the TOA imbalance minus the control simulation divided by the injection amount in Tg S to investigate linearity. The TOA imbalance per Tg S injection is reduced in most cases with increasing injection amount. The strongest decrease occurs for the high-altitude injection cases (dashed lines and open symbols), in correlation with the strongest decrease in AOD per Tg S injection with emission amount (Table 4 and Figure 12, top row). The largest reduction in radiative TOA imbalance from the control simulation is reached for the 15°S high-altitude injection case and is about 15–30% larger (depending on the injection amount) than what can be achieved with the injection at the equator (Figure 12, top row). These differences are, however, within the range of uncertainties due to natural variability. In addition, the 15°N injection case shows slightly larger and the 30°S injection case shows comparable changes to the injections at the equator. For low-altitude injection cases, the injections at the equator and the 15°S injection case show similar values in AOD changes per injection amount, while the 15°N and both 30°N and 30°S injection cases are less effective.

Surface temperature changes per injection amount decrease for most cases with increasing injection amount, similar to what is found for the TOA imbalance (Table 5). However, for low-altitude injections at 15°N, 15°S, and 30°S, surface temperatures per injection amount increase. The increasing efficiency of the surface temperature reduction per injection amount is larger in the NH than in the SH, despite the fact that the efficiency of TOA imbalance is larger in the SH than in the NH. As pointed out in section 4.1, extra cooling in the NH may be achieved due to the recovery of the Arctic sea ice and by the difference in land versus ocean area which provides a different heat capacity. Also, less cooling of the Southern Ocean occurs due to the short period of the experiment, while faster cooling is expected over land. For 12 Tg SO₂/yr injections at the equator,

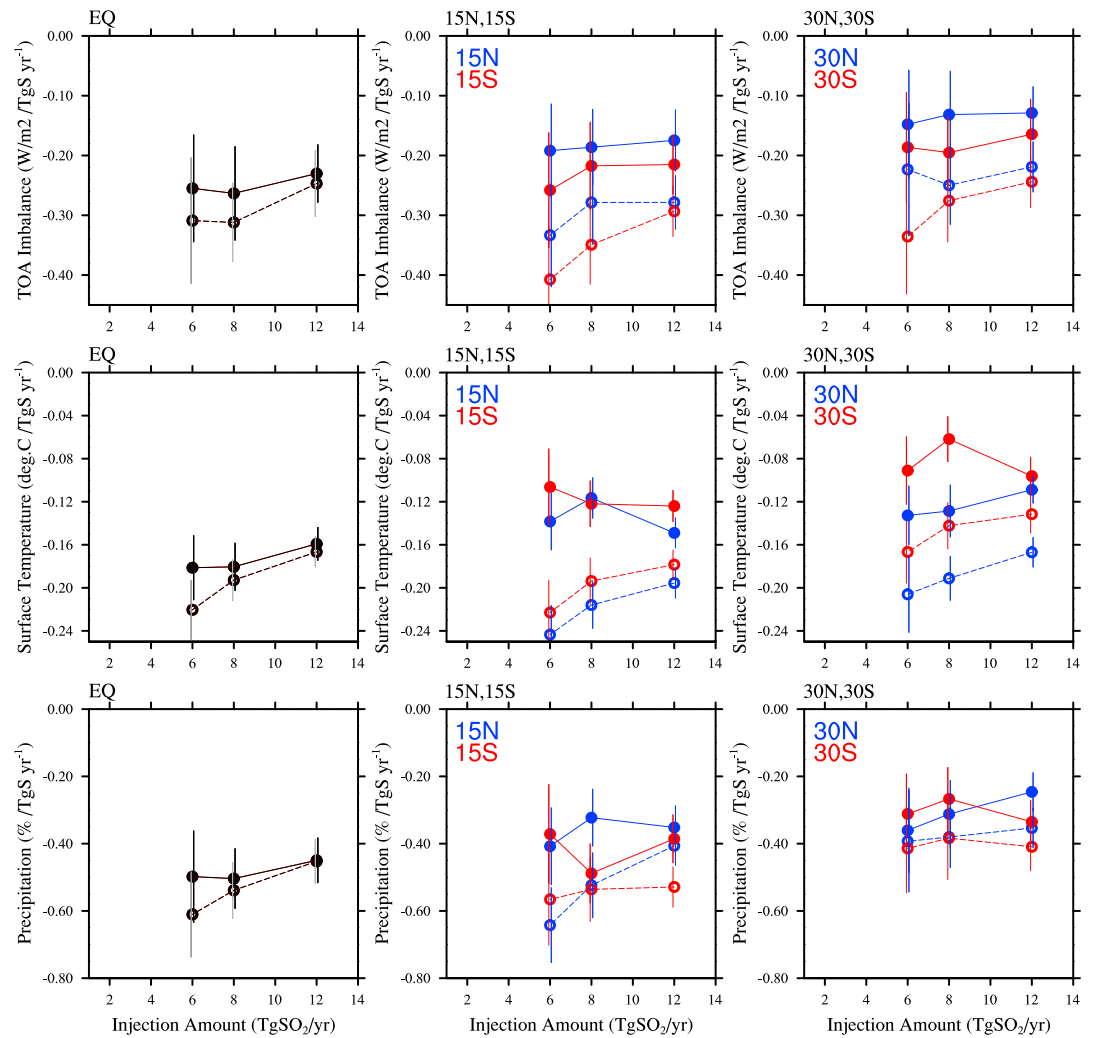


Figure 12. Annually and globally averaged (top row) TOA imbalance, (middle row) surface temperature, and (bottom row) precipitation, minus the control, and divided by the injection amount, shown for different injection amounts and for different injection altitudes, 1 km above the tropopause (solid lines and filled circles) and 5 km above the tropopause (dashed lines and open circles), and for different injection locations, (left column) equator, (middle column) 15°N and 15°S, and (right column) 30°N and 30°S. Error bars indicate the uncertainty due to natural variability in both the injection and control simulations.

Table 4

Top of the Atmosphere Imbalance (in W/m^2 per $Tg\ S/yr$) With Injection Latitude, Derived Between 2043 and 2049

Altitude	Injection	50°S	30°S	15°S	Equator	15°N	30°N	50°N
30 hPa	6 $Tg\ SO_2$	0.16 ± 0.08	0.34 ± 0.09	0.41 ± 0.09	0.31 ± 0.11	0.33 ± 0.09	0.15 ± 0.09	0.11 ± 0.10
30 hPa	8 $Tg\ SO_2$	0.15 ± 0.07	0.28 ± 0.06	0.35 ± 0.07	0.31 ± 0.07	0.29 ± 0.07	0.13 ± 0.07	0.11 ± 0.07
30 hPa	12 $Tg\ SO_2$	0.13 ± 0.04	0.24 ± 0.06	0.29 ± 0.04	0.25 ± 0.06	0.29 ± 0.05	0.13 ± 0.03	0.12 ± 0.05
60 hPa	6 $Tg\ SO_2$	0.17 ± 0.10	0.19 ± 0.10	0.26 ± 0.10	0.26 ± 0.09	0.19 ± 0.08	0.22 ± 0.11	0.02 ± 0.08
60 hPa	8 $Tg\ SO_2$	0.15 ± 0.07	0.20 ± 0.07	0.22 ± 0.07	0.26 ± 0.08	0.19 ± 0.06	0.25 ± 0.07	0.05 ± 0.06
60 hPa	12 $Tg\ SO_2$	0.10 ± 0.04	0.16 ± 0.04	0.22 ± 0.05	0.23 ± 0.05	0.18 ± 0.05	0.22 ± 0.04	0.05 ± 0.04

Note. The listed uncertainty of the values is due to natural variability in both the injection and control simulations.

Table 5*Surface Temperature Reduction in K per Tg S/yr, With Injection Latitude, Derived Between 2043 and 2049*

Altitude	Injection	50°S	30°S	15°S	Equator	15°N	30°N	50°N
30 hPa	6 Tg SO ₂	0.05 ± 0.03	0.17 ± 0.03	0.22 ± 0.03	0.22 ± 0.03	0.24 ± 0.03	0.21 ± 0.04	0.11 ± 0.03
30 hPa	8 Tg SO ₂	0.06 ± 0.02	0.14 ± 0.02	0.19 ± 0.02	0.19 ± 0.02	0.22 ± 0.02	0.19 ± 0.02	0.13 ± 0.02
30 hPa	12 Tg SO ₂	0.06 ± 0.01	0.13 ± 0.02	0.18 ± 0.01	0.17 ± 0.01	0.20 ± 0.01	0.17 ± 0.01	0.10 ± 0.02
60 hPa	6 Tg SO ₂	0.06 ± 0.03	0.09 ± 0.03	0.11 ± 0.04	0.18 ± 0.03	0.15 ± 0.03	0.13 ± 0.01	0.03 ± 0.01
60 hPa	8 Tg SO ₂	0.05 ± 0.03	0.06 ± 0.02	0.12 ± 0.02	0.18 ± 0.02	0.12 ± 0.02	0.12 ± 0.04	0.02 ± 0.01
60 hPa	12 Tg SO ₂	0.05 ± 0.02	0.10 ± 0.02	0.12 ± 0.02	0.16 ± 0.02	0.14 ± 0.01	0.11 ± 0.04	0.01 ± 0.01

Note. The listed uncertainty of the values is due to natural variability in both the injection and control simulations.

surface temperature changes do not differ significantly, independently of the injection altitude, despite some differences in AOD. The strongest cooling per injection amount is achieved for high-altitude injections at 15°N and 15°S, aligned with the strongest reduction in TOA imbalance. Interestingly, for low-altitude injections of 12 Tg SO₂/yr, the difference in temperature changes between injections at the equator and at 15°N are within the uncertainty due to natural variability, despite significant differences in sulfate lifetime and AOD change per injection amount.

Precipitation changes are influenced by both change in energy flux and surface temperature. A reduction in short-wave downwelling radiation changes the latent heat flux and therefore results in reduced global precipitation (e.g., Bala et al., 2010; Tilmes et al., 2013), while increasing temperatures will result in increasing global precipitation. Since temperature efficiencies with increasing injection amount respond differently for NH and SH injection locations, precipitation changes show a mixed signal for those cases (Figure 12, bottom row).

5. Discussion and Conclusions

Forty-two single-point injection experiments were performed using the fully coupled Earth system model, CESM1(WACCM), to explore the sensitivity of stratospheric aerosol mass, AOD, and climate to stratospheric SO₂ injection location. We find that single-point injections outside the equator are more efficient in reducing global temperatures than injections at the equator for high-altitude injections (at about 5 km above the tropopause) and equally efficient for high-altitude injections at 30°S. For injections at 25 km at the equator, sulfate burden is mostly contained in the tropics. For high-altitude injections at 15°N and 15°S, both SO₂ and sulfate are more effectively transported outside the tropics and toward middle and high latitudes, which results in a smaller effective radius at the injection location than for injections at the equator. For injection locations farther poleward, here 30°N and 30°S, SO₂ and sulfate aerosol remain mostly outside the tropics and accumulate in middle and high latitudes. Injections at 50°N and 50°S result in much less stratospheric sulfate burden, since most of the SO₂ is injected in the downwelling branch of the BDC, which removes gas and aerosol particles quickly from the stratosphere.

We find that largest surface cooling per injection amount can be achieved for high-altitude injection locations at 15°N and 15°S instead of at the equator. Global surface temperature reductions of 0.16–0.17 ± 0.02° per Tg S/yr injection for 12 Tg S/yr injection could be archived for both high- and low-altitude injections at the equator over a 10 year experiment, averaging the last 7 years of the simulation. Injections at 15°N and 15°S and at 25 km altitude resulted in temperature reduction of 0.20 ± 0.01 and 0.18 ± 0.01° per Tg S/yr injection, respectively, and 0.17 ± 0.01° per Tg S/yr injection at 30°N and at 22 km. Since these results are based on 10 year simulations further cooling would be expected in longer simulations since temperatures are not in steady state at that time (see Figure A2 and MacMartin et al., 2017). Simultaneous injections at 25 km and at both 15°N and 15°S with each 12 Tg SO₂/yr were shown to lead to changes in AOD of 0.032 per Tg S/yr compared to injections at the equator with 24 Tg SO₂/yr that lead to changes in AOD of 0.026 per Tg S/yr (MacMartin et al., 2017). This supports our findings that injections outside the equator at 25 km are more efficient to change AOD and therefore also temperature than at the equator.

In general, SO₂ injections at high altitudes are more efficient in increasing aerosol burden in the stratosphere, which is in agreement with earlier studies (English et al., 2012; Niemeier et al., 2011). Injections at 5 km above the tropopause produce about 50% more aerosol mass, which is mostly located in the tropics. However, in contrast to earlier studies, AOD differences between the high and low injection cases are smaller than changes

in aerosol mass because of differences in the effective radius. Transport toward midlatitudes is also more efficient in the low-altitude injection case. This results in similar AOD and surface temperature change for injections of 12 Tg SO₂ at the equator for both injection altitudes. Besides, injections at low altitudes are likely cheaper using aircraft and injections at the equator are slightly more efficient to reduce temperatures than outside the equator for the investigated injection amounts.

Changes in transport and stratospheric temperatures between the different injection cases also cause changes in the QBO. A detailed investigation of these changes for high-altitude injection cases is discussed in Richter et al. (2017). For equatorial injections, the QBO does show a prolonging westerly phase, as simulated in earlier studies (Aquila et al., 2014; Pitari et al., 2016; Vioni et al., 2017), and therefore adds to the confinement of tracers within this region. On the other hand, our simulations show that the QBO period can decrease for injections away from the equator (Richter et al., 2017). Besides, differences in aerosol distribution and stratospheric temperatures for low- and high-altitude injection cases impacts stratospheric water vapor and ozone differently. These questions will be explored in a future study.

In comparison to earlier studies, stratospheric sulfate lifetime (sulfate burden per injection amount) is slightly higher in our simulations. SO₂ injections at the equator result in stratospheric sulfate burden of about 6.6 Tg S per 6 Tg S/yr injections at around 20 km (60 hPa), while Niemeier and Timmreck (2015) and English et al. (2012) report sulfate burden of around 6 Tg S for 10 Tg S/yr injections at a similar injection location. Differences may be a result of the smaller injection amount tested compared to earlier studies. Also, differences are possible due to the larger complexity in our model, including interactions between aerosols, chemistry, radiation, and climate, resulting in a larger stratospheric aerosol lifetime (Mills et al., 2017). In terms of TOA radiative imbalance for injections at 60 hPa at the equator, Niemeier and Timmreck (2015) reported a forcing efficiency of around 0.2 W/m² per Tg S/yr injection (for injection amounts up to 10 Tg S/yr), which is similar to our result of 0.22 Tg S per Tg S/yr injection for up to 6 Tg S injection amount.

Injections at 15°N and 15°S and at 5 km (30 hPa) above the tropopause result in a forcing efficiency of 0.28 W/m² per Tg S/yr for injections of 12 Tg SO₂/yr, which is an increase in forcing efficiency by over 25% compared to injections at the equator. Pierce et al. (2010) and Benduhn et al. (2016) further considered the injection of H₂SO₄ in addition or instead of using SO₂, in order to better control the particle size. The prevalence of smaller particles in the stratosphere would allow an even more efficient radiative forcing reduction with injection amount.

Based on these findings, the combination of injection locations outside the equator allows one to change the stratospheric aerosol distribution in a controlled way and, with that, AOD and surface climate (Kravitz et al., 2017; MacMartin et al., 2017). Improved adjustments of the aerosol mass distribution and AOD may be possible by varying the location and timing of injections aligned with the location of the divergence of the stream functions of the BDC and considerations of large-scale mixing and transport barriers. Since the TOA imbalance and temperature changes are not directly correlated to AOD changes, and therefore to shortwave radiative forcing, considering transport characteristics of the stratosphere for identifying injection regions may be more efficient than following the maximum intensity of solar radiation, as suggested by Laakso et al. (2017).

However, due to the long lifetime of sulfate, the aerosol distribution is controlled by stratospheric transport, which limits the ability to perfectly manipulate the location of aerosols in the stratosphere. In addition to the single-point injection experiment described here, combined injection experiments are required if more than one injection location would be considered for climate engineering. Finally, SO₂ emissions into a certain location may translate into a different aerosol distribution using a model with different transport characteristics. Even if the same aerosol distribution would be used in a different model, as suggested by Tilmes et al. (2015), resulting changes in radiative forcing and temperature pattern may be strongly model dependent and have to be therefore explored in multimodel comparison studies.

Appendix A

The appendix contains additional figures to support the discussion in the main text. Figure A1 is similar to Figure 1 but illustrates additional injection cases to visualize differences in the injection amount. Figure A2 shows the annual evolution of global mean AOD and surface air temperature to justify the averaging period between years 2 and 9 for AOD and between years 3 and 9 for surface air temperature, as used

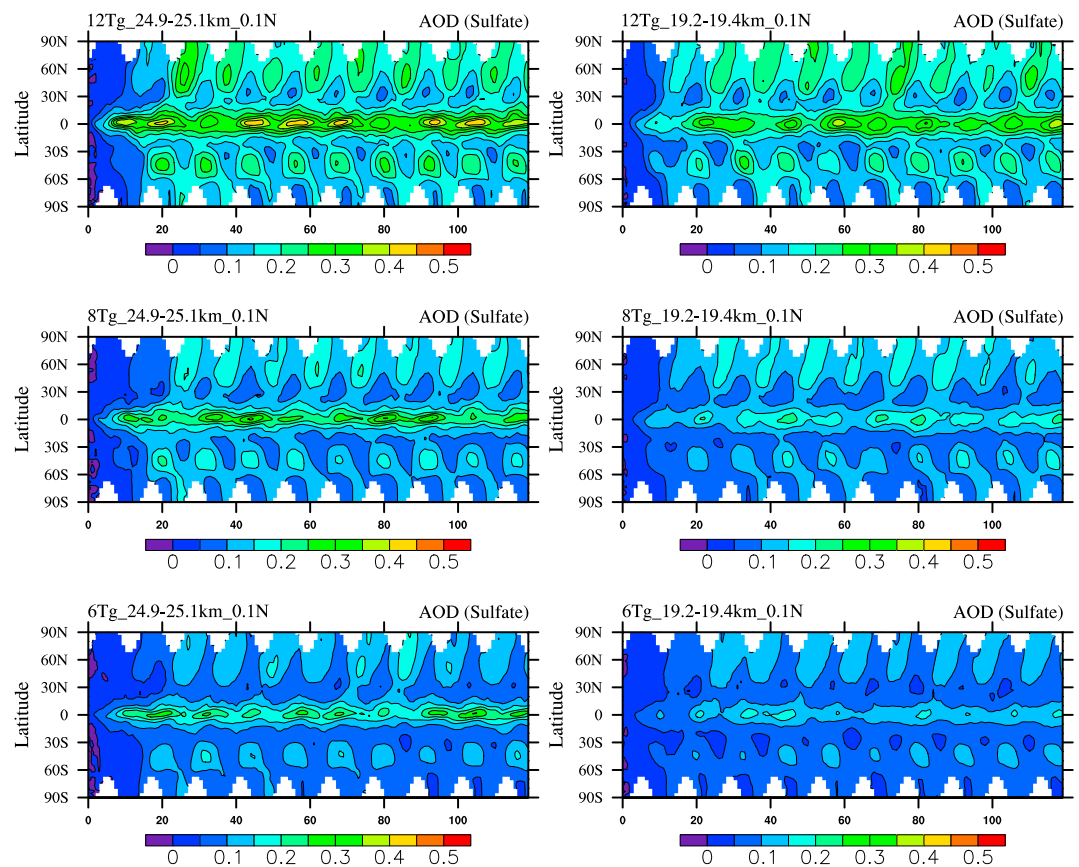


Figure A1. Aerosol optical depth in the visible (550 nm) from stratospheric sulfate for the equatorial SO₂ injection simulations minus the control as a function of time (in months) for different injection amounts, (top row) 12 Tg SO₂/yr, (middle row) 8 Tg SO₂/yr, and (bottom row) 6 Tg SO₂/yr and injection altitude (left column) 5 km above the tropopause, 30 hPa and (right column) 1 km above the tropopause, 60 hPa.

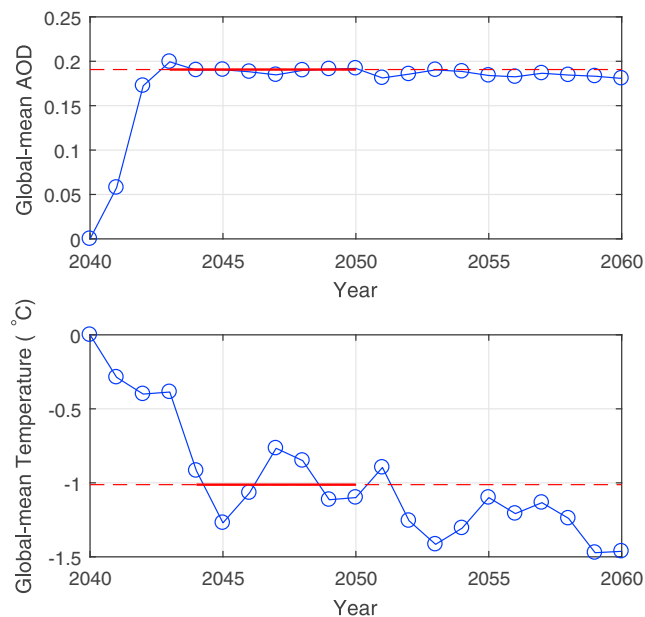


Figure A2. Annual and global mean (top) AOD and (bottom) surface air temperature for the 12 Tg SO₂/yr equatorial SO₂ injection simulation, between 2040 and 2059. Dashed lines indicate the average between 2042–2029 (Figure A2, top) and 2043–2049 (Figure A2, bottom). The averaged period is also marked as a solid red line.

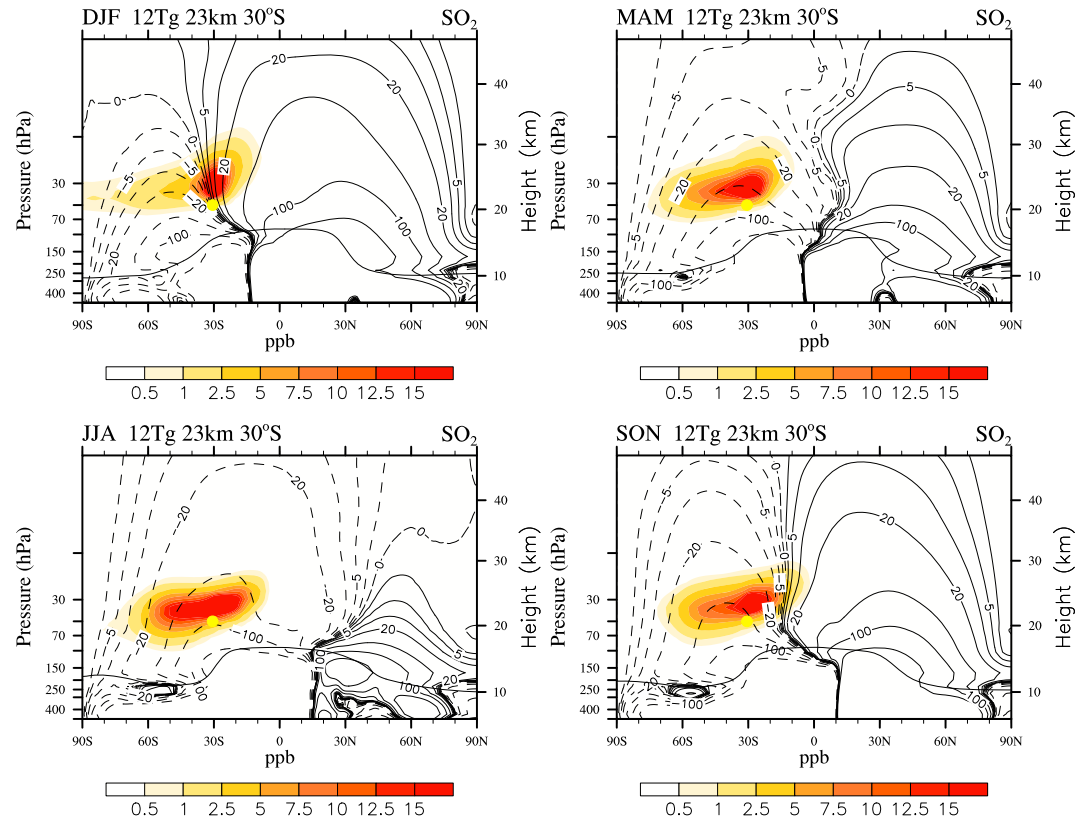


Figure A3. Same as Figure 2 but for continuous injections of 12 Tg SO₂/yr at 23 km altitude at 30°S.

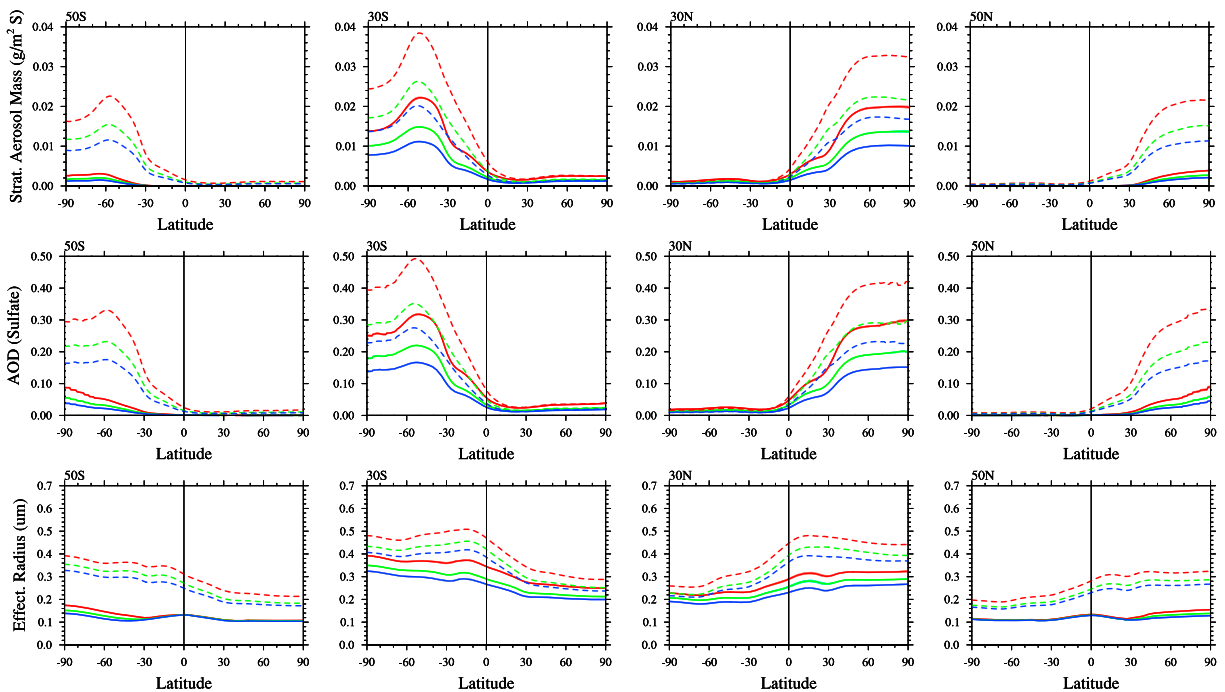


Figure A4. Same as Figure 8 but for different injection locations, (first column) 50°S, (second column) 30°S, (third column) 30°N, and (fourth column) 50°N.

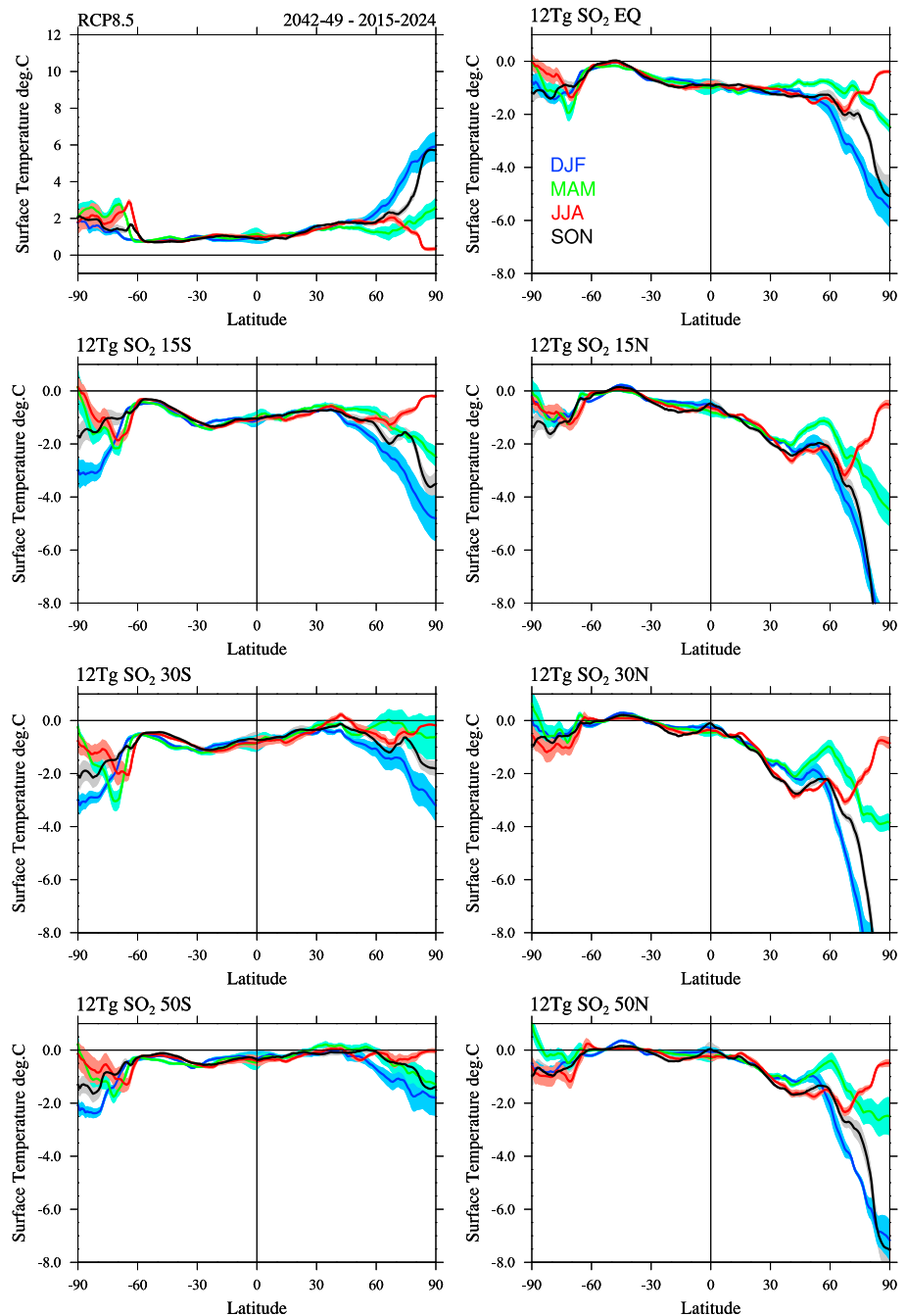


Figure A5. Seasonal zonal averaged surface temperature averaged between 2042 and 2049 for the (top left panel) control simulation and (other panels) surface temperature differences from the control for continuous 12 Tg SO₂/yr injections at different injection locations (different panels); December–February (DJF) (blue), March–May (MAM) (green), June–August (JJA), (red), and September–November (SON) (black). Variability within different years in terms of standard deviation is indicated as shaded regions around the lines.

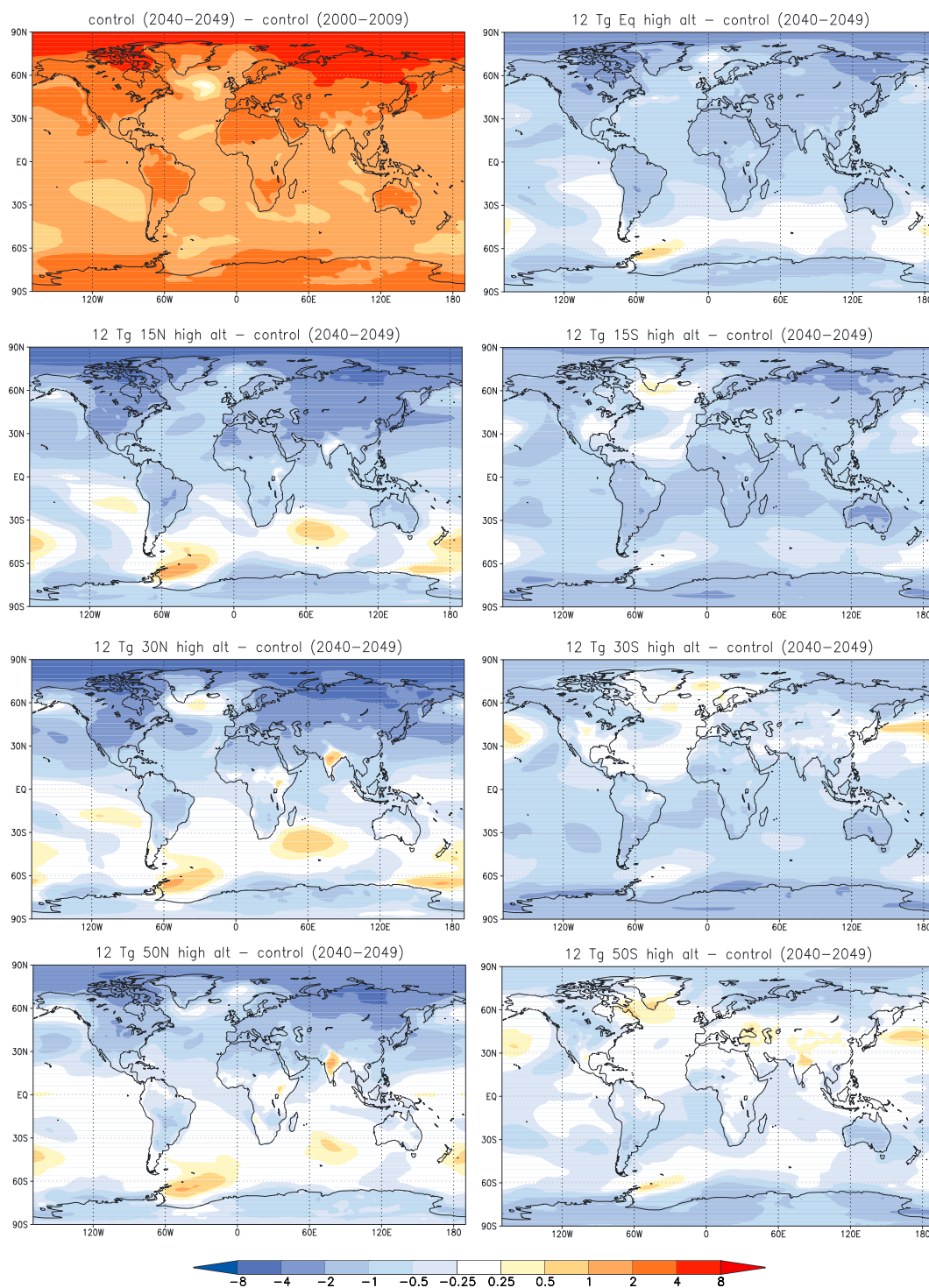


Figure A6. Maps of surface temperature differences between the continuous 12 Tg SO₂/yr injections at different injection locations (different panels) averaged between 2040 and 2049 and the control (averaged between 2000 and 2009). Values greater in magnitude than 0.5°C are statistically significant at the 95% confidence level as calculated by a two-sample unpaired Student’s *t* test.

in the main text. Figure A3 is similar to Figure 2; however, it shows the outcome of a different injection location, namely, at 30°S. Figure A4 is similar to Figure 8 but also illustrates the result of injections at additional locations, as investigated in the study. Figure A5 shows the seasonal change in zonally averaged surface temperature. This information was not added to the main text, since the discussion is mostly focused on annual changes, but is expected to be useful for the reader. Finally, Figure A6 adds information on regional response of surface temperature changes between 2040–2049 and 2000–2009 (left column, top) and the response to SO₂ injections of 12 TgSO₂/yr at different locations between 2040 and 2049.

Acknowledgments

We thank Anne Sasha Glanville, Anne K. Smith, Ulrike Niemeier, and three anonymous reviewers for useful comments and suggestions. We further would like to acknowledge high-performance computing support from Yellowstone (ark:/85065/d7wd3xhc) provided by NCAR's Computational and Information Systems Laboratory, sponsored by the National Science Foundation. The Pacific Northwest National Laboratory is operated for the U.S. Department of Energy by Battelle Memorial Institute under contract DE-AC05-76RL01830. The CESM project is supported by the National Science Foundation and the Office of Science (BER) of the U.S. Department of Energy. The National Center for Atmospheric Research is funded by the National Science Foundation. This research was developed with funding from the Defense Advanced Research Projects Agency (DARPA). The views, opinions, and/or findings expressed are those of the author and should not be interpreted as representing the official views or policies of the Department of Defense or the U.S. Government. All simulations were carried out on the Yellowstone high-performance computing platform (Computational and Information Systems Laboratory, 2012) and are available to the community via the Earth System Grid at https://www.earthsystemgrid.org/dataset/ucar.cgd.cesm4.so2_geong.html.

References

- Andrews, D. G., Holton, J. R., & Leovy, C. B. (1987). *Middle atmosphere dynamics*. San Diego, CA: Academic Press.
- Aquila, V., Oman, L. D., Stolarski, R. S., Colarco, P. R., & Newman, P. A. (2013). Correction to "Dispersion of the volcanic sulfate cloud from a Mount Pinatubo-like eruption". *Journal of Geophysical Research: Atmospheres*, *118*, 7849. <https://doi.org/10.1002/jgrd.50616>
- Aquila, V., Garfinkel, C. I., Newman, P., Oman, L., & Waugh, D. (2014). Modifications of the quasi-biennial oscillation by a geoengineering perturbation of the stratospheric aerosol layer. *Geophysical Research Letters*, *41*, 1738–1744. <https://doi.org/10.1002/2013GL058818>
- Bala, G., Caldeira, K., Nemani, R., Cao, L., Ban-Weiss, G., & Shin, H.-J. (2010). Albedo enhancement of marine clouds to counteract global warming: Impacts on the hydrological cycle. *Climate Dynamics*, *37*(5–6), 915–931. <https://doi.org/10.1007/s00382-010-0868-1>
- Benduhn, F., Schallack, J., & Lawrence, M. G. (2016). Early growth dynamical implications for the steerability of stratospheric solar radiation management via sulfur aerosol particles. *Geophysical Research Letters*, *43*, 9956–9963. <https://doi.org/10.1002/2016GL070701>
- Butchart, N. (2014). The Brewer-Dobson circulation. *Reviews of Geophysics*, *52*, 157–184. <https://doi.org/10.1002/2013RG000448>
- Committee on Geoengineering Climate (2015). *Climate Intervention: Reflecting Sunlight to Cool Earth, and Carbon Dioxide Removal and Reliable Sequestration*. Washington, DC: National Academies Press.
- Computational and Information Systems Laboratory (2012). Yellowstone: IBM iDataPlex System. Cheyenne, WY: NCAR Strategic Capability Projects.
- Crutzen, P. J. (2006). Albedo enhancements by stratospheric sulfur injections: A contribution to resolve a policy dilemma? An Editorial Essay. *Climate change*, *77*, 211–219.
- English, J. M., Toon, O. B., & Mills, M. J. (2012). Microphysical simulations of sulfur burdens from stratospheric sulfur geoengineering. *Atmospheric Chemistry and Physics*, *12*(10), 4775–4793. <https://doi.org/10.5194/acp-12-4775-2012>
- Garcia, R. R., & Randel, W. J. (2008). Acceleration of Brewer-Dobson circulation due to increase in greenhouse gases. *Journal of the Atmospheric Sciences*, *65*, 2731–2739.
- Garcia, R. R., Smith, A. K., Kinnison, D. E., de la Cámara, Á., & Murphy, D. J. (2017). Modification of the gravity wave parameterization in the whole atmosphere community climate model: Motivation and results. *Journal of the Atmospheric Sciences*, *74*(1), 275–291. <https://doi.org/10.1175/JAS-D-16-0104.1>
- Guenther, A. B., Jiang, X., Heald, C. L., Sakulyanontvittaya, T., Duhl, T., Emmons, L. K., & Wang, X. (2012). The Model of Emissions of Gases and Aerosols from Nature version 2.1 (MEGAN2.1): An extended and updated framework for modeling biogenic emissions. *Geoscientific Model Development*, *5*(6), 1471–1492. <https://doi.org/10.5194/gmd-5-1471-2012>
- Haywood, J. M., Jones, A., Bellouin, N., & Stephenson, D. (2013). Asymmetric forcing from stratospheric aerosols impacts Sahelian rainfall. *Nature Climate Change*, *3*(7), 660–665.
- Heckendorn, P., Weisenstein, D., Fueglistaler, S., Luo, B. P., Rozanov, E., Schraner, M., ... Peter, T. (2009). The impact of geoengineering aerosols on stratospheric temperature and ozone. *Environmental research letters*, *4*, 45108. <https://doi.org/10.1088/1748-9326/4/4/045108>
- Hommel, R., & Graf, H.-F. (2011). Modelling the size distribution of geoengineered stratospheric aerosols. *Atmospheric Science Letters*, *12*(2), 168–175. <https://doi.org/10.1002/asl.285>
- Kay, J. E., Deser, C., Phillips, A., Mai, A., Hannay, C., Strand, G., ... Vertenstein, M. (2015). The community Earth system model (CESM) large ensemble project: A community resource for studying climate change in the presence of internal climate variability. *Bulletin of the American Meteorological Society*, *96*(8), 1333–1349. <https://doi.org/10.1175/BAMS-D-13-00255.1>
- Kravitz, B., MacMartin, D. G., Mills, M. J., Richter, J. H., Tilmes, S., Lamarque, J.-F., ... Vitt, F. (2017). First simulations of designing stratospheric sulfate aerosol geoengineering to meet multiple simultaneous climate objectives. *Journal of Geophysical Research: Atmospheres*, *122*. <https://doi.org/10.1002/2017JD026874>
- Laakso, A., Korhonen, H., Romakkaniemi, S., & Kakkola, H. (2017). Radiative and climate effects of stratospheric sulfur geoengineering using seasonally varying injection areas. *Atmospheric Chemistry and Physics*, *17*, 6957–6974. <https://doi.org/10.5194/acp-17-6957-2017>
- MacMartin, D. G., Kravitz, B., Tilmes, S., Richter, J. H., Mills, M. J., ... Vitt, F. (2017). The climate response to stratospheric aerosol geoengineering can be tailored using multiple injection locations. *Journal of Geophysical Research: Atmospheres*, *122*. <https://doi.org/10.1002/2017JD026868>
- Marsh, D. R., Mills, M. J., Kinnison, D. E., Lamarque, J.-F., Calvo, N., & Polvani, L. M. (2013). Climate Change from 1850 to 2005 Simulated in CESM1 (WACCM). *Journal of Climate*, *26*(19), 7372–7391. <https://doi.org/10.1175/JCLI-D-12-00558.1>
- McCusker, K. E., Battisti, D. S., & Bitz, C. M. (2015). Inability of stratospheric sulfate aerosol injections to preserve the West Antarctic Ice Sheet. *Geophysical Research Letters*, *42*, 4989–4997. <https://doi.org/10.1002/2015GL064314>
- Meinshausen, M., Smith, S. J., Calvin, K., Daniel, J. S., Kainuma, M. L. T., Lamarque, J.-F., ... Vuuren, D. P. (2011). The RCP greenhouse gas concentrations and their extensions from 1765 to 2300. *Climate Change*, *109*(1–2), 213–241. <https://doi.org/10.1007/s10584-011-0156-z>
- Mills, M. J., Schmidt, A., Easter, R., Solomon, S., Kinnison, D. E., Ghan, S. J., ... Gettelman, A. (2016). Global volcanic aerosol properties derived from emissions, 1990–2014, using CESM1(WACCM). *Journal of Geophysical Research: Atmospheres*, *121*, 2332–2348. <https://doi.org/10.1002/2015JD024290>
- Mills, M. J., Richter, J., Tilmes, S., Kravitz, B., MacMartin, D. G., Glanville, S. A., ... Kinnison, D. E. (2017). Radiative and chemical response to interactive stratospheric sulfate aerosols in fully coupled CESM1(WACCM). *Journal of Geophysical Research: Atmospheres*, *122*. <https://doi.org/10.1002/2017JD027006>
- Morgenstern, O., Hegglin, M., Rozanov, E., O'Connor, F., Luke Abraham, N., Akiyoshi, H., ... Zeng, G. (2017). Review of the global models used within phase 1 of the Chemistry-Climate Model Initiative (CCMI). *Geoscientific Model Development*, *10*(2), 639–671. <https://doi.org/10.5194/gmd-10-639-2017>

- Neale, R. B., Richter, J., Park, S., Lauritzen, P. H., Vavrus, S. J., Rasch, P. J., & Zhang, M. (2013). The mean climate of the community atmosphere model (CAM4) in forced SST and fully coupled experiments. *Journal of Climate*, *26*(14), 5150–5168. <https://doi.org/10.1175/JCLI-D-12-00236.1>
- Niemeier, U., & Timmreck, C. (2015). What is the limit of climate engineering by stratospheric injection of SO₂. *Atmospheric Chemistry and Physics*, *15*(16), 9129–9141. <https://doi.org/10.5194/acp-15-9129-2015>
- Niemeier, U., Schmidt, H., & Timmreck, C. (2011). The dependency of geoengineered sulfate aerosol on the emission strategy. *Atmospheric Science Letters*, *12*(2), 189–194. <https://doi.org/10.1002/asl.304>
- Pierce, J. R., Weisenstein, D. K., Heckendorn, P., Peter, T., & Keith, D. W. (2010). Efficient formation of stratospheric aerosol for climate engineering by emission of condensable vapor from aircraft. *Geophysical Research Letters*, *37*, L18805. <https://doi.org/10.1029/2010GL043975>
- Pitari, G., Aquila, V., Kravitz, B., Robock, A., Watanabe, S., Cionni, I., ... Tilmes, S. (2014). Stratospheric ozone response to sulfate geoengineering: Results from the geoengineering model intercomparison project (geoMIP). *Journal of Geophysical Research: Atmospheres*, *119*, 2629–2653. <https://doi.org/10.1002/2013JD020566>
- Pitari, G., Di Genova, G., Mancini, E., Visionsi, D., Gandolfi, I., & Cionni, I. (2016). Stratospheric aerosols from major volcanic eruptions: A composition-climate model study of the aerosol cloud dispersal and e-folding time. *Atmosphere*, *7*(6), 75. <https://doi.org/10.3390/atmos7060075>
- Plumb, A. R., & Ferrari, R. (2005). Transformed Eulerian-mean theory. Part I: Nonquasigeostrophic theory for eddies on a zonal-mean flow. *Journal of Physical Oceanography*, *35*, 165. <https://doi.org/10.1175/JPO-2669.1>
- Rasch, P. J., Crutzen, P. J., & Coleman, D. B. (2008). Exploring the geoengineering of climate using stratospheric sulfate aerosols: The role of particle size. *Geophysical Research Letters*, *35*, L02809. <https://doi.org/10.1029/2007GL032179>
- Richter, J. H., Tilmes, S., Mills, M. J., Tribbia, J. J., Kravitz, B., MacMartin, D. G., ... Lamarque, J. F. (2017). Stratospheric dynamical response and ozone feedbacks in the presence of SO₂ injections. *Journal of Geophysical Research: Atmospheres*, *122*. <https://doi.org/10.1002/2017JD026912>
- Robock, A., Oman, L., & Stenchikov, G. L. (2008). Regional climate responses to geoengineering with tropical and Arctic SO₂ injections. *Journal of Geophysical Research*, *113*, D16101. <https://doi.org/10.1029/2008JD010050>
- Sakai, T., Uchino, O., Nagai, T., Liley, B., Morino, I., & Fujimoto, T. (2016). Long-term variation of stratospheric aerosols observed with lidars over Tsukuba, Japan, from 1982 and Lauder, New Zealand, from 1992 to 2015. *Journal of Geophysical Research: Atmospheres*, *121*, 10,283–10,293. <https://doi.org/10.1002/2016JD025132>
- Schäfer, S., Lawrence, M., Stelzer, H., Born, W., Low, S., Aaheim, A., ... Vaughan, N. (2015). The European Transdisciplinary Assessment of Climate Engineering (EuTRACE): Removing Greenhouse Gases from the Atmosphere and Reflecting Sunlight away from Earth. Final Report of the FP7 CSA project EuTRACE. Funded by the European Union's Seventh Framework Programme under Grant Agreement 306993. Potsdam: Institute for Advanced Sustainability Studies (IASS). <https://doi.org/10.2312/iass.2015.024>
- Shuckburgh, E., Norton, W. A., Iwi, A. M., & Haynes, P. (2001). Influence of the quasi-biennial oscillation on isentropic transport and mixing in the tropics and subtropics. *Journal of Geophysical Research*, *106*, 14,327–14,337.
- Tilmes, S., Garcia, R. R., Kinnison, D. E., Gettelman, A., & Rasch, P. J. (2009). Impact of geoengineered aerosols on the troposphere and stratosphere. *Journal of Geophysical Research*, *114*, D12305. <https://doi.org/10.1029/2008JD011420>
- Tilmes, S., Fasullo, J., Lamarque, J.-F., Marsh, D. R., Mills, M., Alterskjaer, K., ... Watanabe, S. (2013). The hydrological impact of geoengineering in the Geoengineering Model Intercomparison Project (geoMIP). *Journal of Geophysical Research: Atmospheres*, *118*, 11,036–11,058. <https://doi.org/10.1002/jgrd.50868>
- Tilmes, S., Jahn, A., Kay, J. E., Holland, M., & Lamarque, J.-F. (2014). Can regional climate engineering save the summer Arctic sea ice? *Geophysical Research Letters*, *41*, 880–885. <https://doi.org/10.1002/2013GL058731.1>
- Tilmes, S., Mills, M. J., Niemeier, U., Schmidt, H., Robock, A., Kravitz, B., ... English, J. M. (2015). A new Geoengineering Model Intercomparison Project (GeoMIP) experiment designed for climate and chemistry models. *Geoscientific Model Development*, *8*(1), 43–49. <https://doi.org/10.5194/gmd-8-43-2015>
- Visioni, D., Pitari, G., & Aquila, V. (2017). Sulfate geoengineering: A review of the factors controlling the needed injection of sulfur dioxide. *Atmospheric Chemistry and Physics*, *17*(6), 3,879–3,889. <https://doi.org/10.5194/acp-17-3879-2017>